ABSOLUTE BREMSSTRAHLUNG YIELDS: 53 keV ELECTRONS ON GOLD

by

SCOTT CHARLES WILLIAMS

Bachelor of Science, 2002
University of North Texas
Denton, Texas

Master of Science, 2003
University of Texas at Dallas
Richardson, Texas

Submitted to the Graduate Faculty of the
College of Science and Engineering
Texas Christian University
in partial fulfillment of the requirements
for the degree of

Doctor of Philosophy

August 2007

ACKNOWLEDGEMENTS

The author would like to thank Dr. C. A. Quarles for his guidance, help, and patience during the development of this dissertation. He would also like to thank Keith Hayton, Ryan Haygood, and David Yale for their help, as well.

TABLE OF CONTENTS

LIST OF FIGURES

LIST OF TABLES/CHARTS

I. Introduction

1.1 Explanation of Processes and a Brief Survey of Relevant Experiments

Despite the relatively long history of the study of bremsstrahlung, it wasn't until recently that it was known that there were several different processes contributing to the continuous bremsstrahlung spectrum. Over the years, there have been many experimental and theoretical studies, as well as reviews [Amusia, 2006; Korol et al., 2002; Pratt et al., 1995; Quarles, 2000], dedicated to the subject, but it wasn't until the 1970s that polarizational bremsstrahlung (and the various types of polarizational bremsstrahlung) was discussed alongside normal bremsstrahlung (sometimes referred to as "ordinary bremsstrahlung"). Normal bremsstrahlung results from electron acceleration (or deceleration, rather) due to target-atom/electron collisions, when scattered in the Coulomb field of the target atom. Basically, as the incident electron is scattered by the target, it loses energy and emits a photon (or photons, possibly) with a maximum energy equal to the incident electron's energy. It is now realized, however, that we need to include polarizational bremsstrahlung contributions to achieve a more complete understanding of the processes involved. Polarizational bremsstrahlung results from the acceleration of electrons in the target-atoms due to the electric field contributions of the incident electrons. The polarizational bremsstrahlung contribution stems from the acceleration of the target-atom's electrons due to repulsion from the incident electron, but radiation as a result of the acceleration of the incident electron and target-atom's nucleus due to electromagnetic attraction (usually considered to be negligible due to the nucleus/electron mass ratio) and Cherenkov radiation are sometimes referred to as polarizational bremsstrahlung as well.

While polarizational contributions to the bremsstrahlung spectra have been demonstrated for electrons incident on gas targets [Portillo et al., 2003], polarizational bremsstrahlung contributions for solid targets remain much more elusive. There are only two documented cases (known to this author) of thin-film polarizational bremsstrahlung, and both of them can be considered to be special cases.

The first case demonstrated a polarizational bremsstrahlung contribution when the energy of the incident electron was near core-level excitation thresholds in metallic Ba, La, and Ce. The paper [Wendin et al., 1977] studied the resonant bremsstrahlung process in the 3d threshold region of the metallic films, thus the energies involved in the study were relatively low (~ 850 eV). Similar (and much more extensive) experiments have also been conducted by a group in the Ukraine [Verkhovtseva et al., 2006], and with gas targets.

The results of a second case of a polarizational contribution for thin-film targets were published by a group in Japan [Ishii, 2006]. Using a “thin” Au target, polarizational bremsstrahlung contributions were demonstrated when the target was bombarded with 1.5 MeV protons at an angle of 90 degrees. Their theoretical work indicates that the main contribution of the continuous x-rays is from polarizational bremsstrahlung due to M-shell electrons (it should be noted that characteristic x-rays from M or higher shells are not reproduced by the Monte Carlo simulation program that we will discuss shortly [Salvat et al., 2006]). The arguments for polarizational bremsstrahlung contributions to the thin-film spectra aren’t entirely convincing, and they admit that their theory overestimates their experimental data by one order of magnitude in the low x-ray region.

It should be noted that both of these experiments were for situations were the theoretical polarizational bremsstrahlung contribution was at a maximum, while the normal bremsstrahlung contribution was at a minimum. The first studies were done with energies in the region of giant atomic resonances, and the second study used heavy particles (the incident protons) in order to suppress normal bremsstrahlung. The research presented in this paper, on the other hand, searched for polarizational bremsstrahlung contributions in experiments dominated by normal bremsstrahlung contributions.

In contrast to the aforementioned studies, a paper published by a group here at Texas Christian University [Portillo et al., 1999] presented data that demonstrated no discernable polarizational contribution for solid-film bremsstrahlung with electrons. The paper suggests that the single-interaction model on which its theoretical calculations are based may not be adequate in describing the polarizational bremsstrahlung effect. The polarizational effect, naturally, is a "collective or many-bodied effect that depends not only on the properties of the incident charged projectile, but significantly on the interaction with the neighboring atoms in the solid which are, of course, also polarized by the projectile" [Portillo et al., 1999]. Thus, the paper hints at the possibility that the polarizational effect might be suppressed due to the so-called "screening effect" on single target-atom due to its interaction with neighboring atoms in the solid.

1.2 Review of Previous Work

Prior to the experimental work that will be presented later in this paper, our experiments had suffered from a variety of problematic issues.

Firstly, initial results presented (and published [Williams et al., 2006]) weren't normalized according to charge collection, rather they were normalized by the amount of time it took to perform the experiments. This was due to the fact that we hadn't yet designed or constructed a decent charge-collector, and were simply trying to get rough data to study. The tungsten filaments' sometimes-erratic thermionic emission characteristics meant that the time/charge ratio wasn't constant, and that the results were probably a little more "rough" than we anticipated. Later research utilized a charge-collector set-up with less-than-ideal features (lots of "leaks" and a possible problem with a coating on the aluminum interior), however the new charge-collector is far less problematic and allows us to make consistent and accurate charge measurements.

Secondly, previous results [Williams et al., 2007] obtained using computer simulations weren't angle-specific, and we had to compare experimental data obtained at ~ 90 or 135 degrees to simulated data that represented radiation produced from 0 to 180 degrees. We are now able to present Monte Carlo simulation data that is angle-specific and this is crucial, considering that both the magnitude and shape of the bremsstrahlung spectrum is angle-dependent.

Thirdly, uncertainties in individual factors used to calculate/measure doubly-differential cross-sections in past experiments prevented us from being able to present cross-section numbers with much confidence. The uncertainties in solid angle, target-thickness, and the number of incident electrons are now much lower than in previous experimental work, and this results in significantly-decreased error in our doubly-differential cross-section calculations/measurements.

Finally, our previous experimental results were also presented without background radiation subtracted [Williams et al., 2006]. This background radiation can be either natural, or radiation produced as a result of "stray" electrons that weren't accurately aimed at the target film. Natural (time-dependent) background radiation rates can be estimated by measuring the natural background for twenty four hours, while stray-electron radiation (which is charge-dependent) can be estimated by inserting a blank aluminum target frame in place of a target film and comparing the resultant radiation detected to the amount of charge measured by the charge-collector. All background runs for stray-electron background resulted in relatively low background counts, and special care was taken to ensure that background radiation was minimized for all experiments, but especially for experiments involving thinner films (where background radiation can greatly affect the results). Both natural and stray-electron background radiation have been subtracted from all results presented in this paper.

1.3 Objectives

This study was done with several goals in mind. Firstly, we wanted to take advantage of the recently-developed Monte Carlo code, PENELOPE, and compare its generated data with our experimental data, with the hope that any discrepancies between the two might indicate possible polarizational bremsstrahlung contributions. Ratios of data for different target-thicknesses were compared with the corresponding ratios obtained using PENELOPE, which is based on the normal bremsstrahlung predictions of Kissel, Quarles, and Pratt [Kissel et al., 1983]. Any variations in structure or magnitude between the experimental ratios and the theoretical ratios could indicate possible

polarizational bremsstrahlung contributions (with ratio comparisons, we have the luxury of ignoring factors such as detector efficiencies and solid angle dependencies). Along with the ratio comparisons, we also wanted to compare our experimental data to the data generated by PENELOPE directly. This involved carefully modeling the efficiency of the Ge detector and making accurate solid angle measurements.

The PENELOPE program, developed by a group in Spain [Salvat et al., 2006], provides a basic simulation of bremsstrahlung emission by electrons. PENELOPE, an acronym for "PENetration and Energy Loss of Positrons and Electrons", provides a "Monte Carlo simulation of coupled electron-photon transport" in energy ranges from <1 keV to ~ GeV [Salvat et al., 2001]. The code system basically consists of a series of "FORTRAN subroutines that perform simulation of electron-photon showers in homogeneous materials of arbitrary compositions" [Salvat et al., 2001]. When running the PENELOPE program, the user must specify what material the target is to be made of (gold, in our case), and what the incident particle involved in the collision is to be. (Along with electrons, PENELOPE can also perform photon and positron simulations.) The user also defines the incident particles' initial energy (in eV) and the targets' thicknesses (in cm). As mentioned earlier, our previous work compared experimental data with PENELOPE-generated data that wasn't angle-specific. But since then, we've managed to obtain PENELOPE data that is specific to a solid angle, comparable to our experimental work. It should also be noted that the systematic differences inherent to the PENELOPE simulations at higher energies increase slightly with the target's atomic number, and differences are visible at low energies due to the decrease of the detector efficiency [Salvat et al., 2001].

Our second goal was to take advantage of our new and more accurate method of film-thickness measurement (to be explained in detail in a later section), and observe the transition from thin to thick-film spectra. Thin-target bremsstrahlung is the radiation of a photon in a single electron-atom collision. Thin-target conditions require that the target be thin enough that the probability for multiple interactions (and significant energy loss) is small as the electrons travel through the target. Thick-target bremsstrahlung is the radiation from multiple interactions when the incident electron is stopped completely by the target film or loses a significant portion of its energy. It is dependent upon many factors including the thin-target cross-section, the electron's energy loss, and the effect of secondary electrons produced in the target. Thus, thick-target bremsstrahlung is better described by a yield than a cross-section [Quarles, 2000]. While studying the target-thickness dependence of bremsstrahlung, we also wanted to investigate the relationship between the target-thicknesses and the angular dependence (thus experiments were performed with radiation measured at 90 and 135 degrees from the beam-line).

The third goal was to obtain cross-section measurements of the two thinnest films (66 and 116 $\mu g/cm^2$) at the aforementioned angles, and compare the measurements with both theoretical predictions and the results of previous studies. In the past, target-thickness measurements had been a dominant source of error in cross-section measurements, and our goal was to take advantage of the reduced uncertainty in the target thicknesses in order to get more accurate doubly-differential cross-section measurements. Previous studies [Ambrose et al., 1987] were also conducted with less-refined experimental set-ups (our improvements will be described later in this paper), and without the advantage of adequate theory that the PENELOPE program provides. With

these facts in mind, it was our aim to obtain the most accurate doubly-differential cross-section measurements for gold targets to date.

II. Experimental Set-up

The set-up used for our experiments is a relatively straight-forward one. A schematic of the set-up can be seen in Figure 1, and a photograph of the equipment in Figure 2.

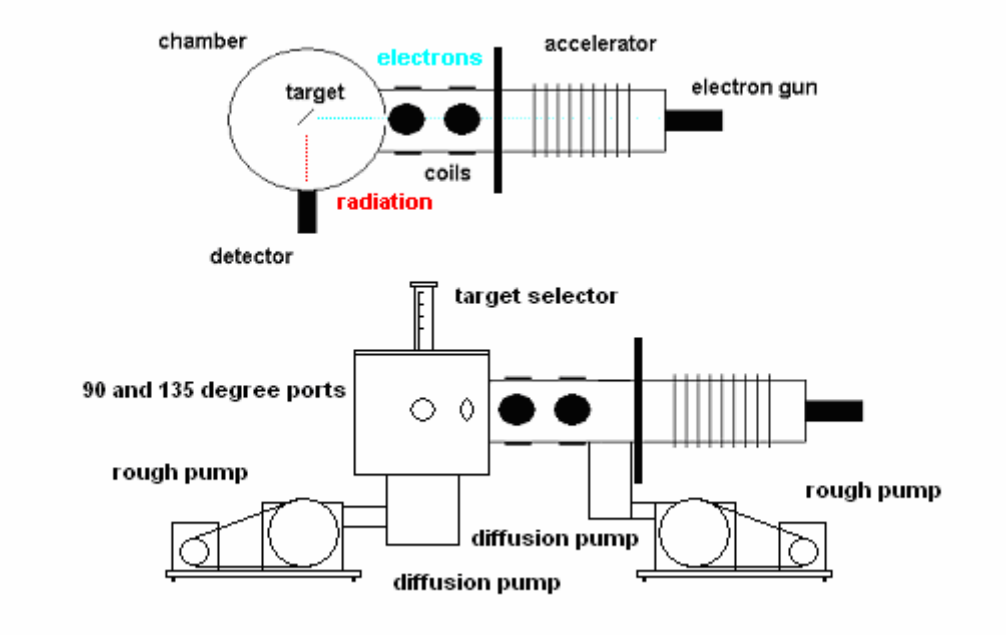

Figure 1 Diagrams of the experimental equipment as seen from above (top) and from the side (bottom) (note: the Ge detector is not shown in the diagram on the bottom

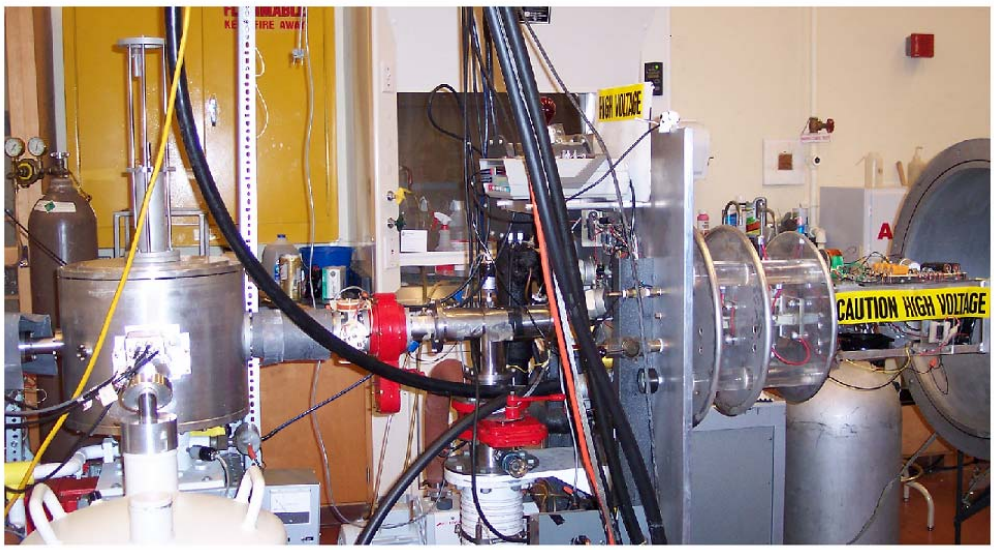

Figure 2 Photograph of the equipment used in the experiments

2.1 Electron Gun

The electron gun used in these experiments produces electrons via thermionic emission from a directly-heated tungsten filament. The filament heater is powered by a 0 to 12 DCV transformer that is controlled by hand, using an insulated knob. All filaments used in the experiments were purchased from Structure Probe Inc., and data sets for each target were made using different filaments, so as to correct for any inconsistencies that each filaments' unique emission characteristics might introduce to the experiments (a difference that was considered to be negligible in the first place).

2.2 Accelerator

The accelerator used in the experiments is a Cockroft-Walton accelerator, and the accelerating voltage is applied in 20 stages by a set of resistors that are set up in a voltage-divider network. The experiments presented in this work were performed using accelerator voltages of approximately 53 keV. The word "approximately" is used because the voltage can drift during experiments, and special care had to be taken to ensure that the voltage remained relatively constant (in other words, the voltage had to be continuously monitored and adjusted during experiments).

2.3 Coils and Collimator

As the electrons travel toward the target chamber, their path is controlled by a LabView program, designed by Sal Portillo. The coils' voltage is tuned so that the charge-collection rate is maximized, and so that the electron beam is aimed near the

center of the target, so as to minimize any bremsstrahlung production due to the aluminum target frame. Thus, tuning the coils' voltage (i.e. aiming the electron beam) involves monitoring both the charge-collection rate, and the resultant radiation detected.

Along with the coils' voltage, a 0.6 cm-diameter Pb collimator (positioned about 10 cm from the target) is employed to ensure that the electron beam hits only the desired target and not the target frame or other targets.

2.4 Target Chamber and Charge-Collector

The target chamber itself is constructed entirely out of aluminum, chosen for its low Z-value, and for machining and durability practicality. When the electrons strike the target atoms, there will be an elastic collision from the Coulomb field. The scattered electrons will strike the chamber wall, and thick-target bremsstrahlung (TTB) will be produced. Thus, a low-Z material (Z=13 for Al) is desirable for chamber fabrication (thick-target bremsstrahlung is proportional to the Z-value of the target). The chamber's wall is 3.3 cm thick, and the chamber has 1 cm-diameter holes at 90 and 135 degrees, so that the radiation can be detected at those angles, and a 5.1 cm-diameter hole at the front of the chamber (where the electrons enter) for the collimator. The .7 cm-thick wall of the charge-collector (also constructed of aluminum) also has holes (1.9 cm-diameter) machined at 90 and 135 degrees, and a 3.2 cm-diameter hole at the front of the collector (again, for the Pb collimator). The collector has both a bottom and top (we tried to give as few opportunities for charge leaks as possible), with a small gap between the wall and top to aid the vacuum pump, and a small hole in the top to allow the target holder to move up and down. The charge-collector is connected with wires to the target-holder, and also to

the isolated portal at the chamber wall (which feeds into the current integrator). The previously-mentioned Pb collimator protrudes out of the hole for the electron beam and into the charge-collector to ensure that the electron-beam is well collimated and that the electrons aren't straying from their intended course. The gap between the outer diameter of the collimator and holes in both the charge collector and the chamber was minimized in order to prevent any charge leak that would prove detrimental to the accuracy of our charge measurements. Because a majority of the electrons end up striking the target or the charge-collector wall directly behind the target (nowhere near any of the aforementioned holes), charge losses are presumed to be negligible.

2.5 Window and Detector

It is possible for the electrons to scatter elastically from the target and travel towards the detector. Thus, when choosing a window for the radiation to pass through, a low-Z material is desirable. This ensures that the window's contribution is minimal. (The extent of the contribution of scattered electron-Kapton window interactions is discussed in greater depth in a later section.) The window must also be transparent to the bremsstrahlung photons produced in the electron-target collisions. Common choices for such a separating window are Mylar and Kapton Polymide. Since the windows were to be exposed to radiation, Kapton was chosen because Mylar is more susceptible to radiation damage.

The radiation was detected using a Princeton Gamma-Tech Ge detector, positioned at either 90 or 135 degrees from the beam-line. The detector was chosen over

a SiLi detector because of its efficiency in the 10 to 60 keV energy range (efficiency details are discussed in detail in Appendix C).

2.6 Other Experimental Equipment

The beam current was measured using an Ortec 581 current integrator, and all data was normalized according to the quantity of charge collected. The computer program, Maestro, was used to record the data for each of the experiments. The Maestro program requires the user to calibrate the radiation energy scale manually, and this was done using an Americium-241 source. The same calibration was used for all of the experimental data presented in this work.

In order to prevent any bremsstrahlung from being produced as a result of air in the target chamber, and in order to assure that there were no radiation absorption problems, all experiments were performed under a vacuum of the order of ~ 10^{-7} torr.

III. Target measurements

The seven targets used in the experiments were all measured using a Fe55 source and the relation:

$$x = - 1/\mu \ln [I(x) / I_o]$$

where x is the target's thickness, μ is the absorption coefficient obtained using the XCOM [XCOM, 2007] and FFAST [FFAST, 2007] internet databases, I_o is the magnitude of the radiation detected with no target in place for a set amount of time, and I(x) is the magnitude of the radiation detected with the target in place for the same set amount of time. All blank measurements used to get a value for I_o were performed within 24 hours of their corresponding target thickness measurements, so as to minimize any error due to source-decay. The half-life of the Fe55 source used is about 2.6 years, so any error due to source-decay is assumed to be negligible.

The target-measurement technique employed greatly increases the accuracy of the thickness measurements, with virtually all of the systematic error originating from the absorption coefficient, μ (whose uncertainty varies from metal to metal). The XCOM and FFAST coefficient values are within 2 or 3 percent agreement, thus it is reasonable to assume that the percent error for the coefficient value is also about 2 or 3 percent.

Both XCOM and FFAST are NIST internet databases, but they were created for different purposes. The XCOM database was developed for radiological physics and dosimetry, while the FFAST database was developed for x-ray diffraction, interferometry, and crystallography. The coefficient values were calculated by different methods for each of the databases, but are usually in relatively good agreement with each

other. Chart 1 displays the advertised and measured thicknesses of each film (using the XCOM coefficient value), as well as uncertainty values.

advertised target thickness ($\mu g/cm^2$)	measured target thickness ($\mu g/cm^2$)	uncertainty ($\mu g/cm^2$)
50	66	2
100	116	4
500	549	17
900	939	28
1130	1295	39
3863	3716	112
28976	N/A	N/A

Chart 1 Comparison of advertised target thickness with measured target thickness and the uncertainty in the measured thickness

All of the gold targets were mounted on aluminum target-holders (each with a hole for the target measuring 1.4 cm in diameter), and all of the targets (except for the 66 and 116 $\mu g/cm^2$ ones) had Graphite Conductive Adhesive 154 (purchased from Electron Microscopy Sciences) applied at the targets' edges for charge-collection purposes. With the exception(s) of the two thickets targets (3716 and 28976 $\mu g/cm^2$), all targets were purchased from MicroMatter and produced using an evaporation technique. The thickest two targets were purchased as rolled foils from Goodfellow Cambridge Limited. Unlike the targets employed in previous experiments carried out by this group, the targets used in this study weren't backed by (~ 15 $\mu g/cm^2$) carbon films for support purposes. This eliminated a source of error (bremsstrahlung produced from the carbon-backing) present in our earlier experiments.

Detailed descriptions of each of the individual targets used in the experiments are provided in Appendix B.

IV. 135 degree results

The first set of data that we'll review is for radiation detected 135 degrees from the electron beam-line. A diagram of the chamber set-up can be seen in Figure 3.

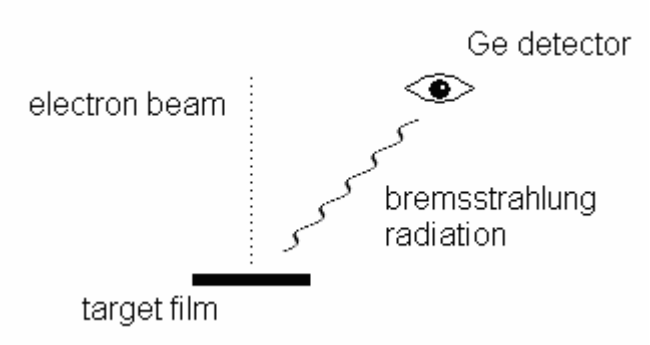

Figure 3 Diagram of the 135 degree geometry used in the experiments

4.1 Spectra

The spectra for all seven targets are shown in Figure 4. The figure gives the (logarithmic) yield (in photons per steradian per keV) for the 66, 116, 549, 939, 1295, 3716, and 28976 $\mu g/cm^2$ targets as a function of photon energy in keV, and the spectra's kinematic end-points are indicative of a 53 keV electron-beam energy. The data for the thinner films (specifically, the 66 and 116 $\mu g/cm^2$ targets) isn't as statistically strong as the data for the other films, and this is why the plots look more "rough" compared to the thick-film plots. The reason for the weaker statistics is that the experiments involving the thin targets require *much* more charge-collection (and, as a result, much more time) than the thick-film experiments to get comparable statistics. As previously stated, all data has been normalized according to charge-collection.

The experimental data in Figure 4 demonstrates several things. We can see that the thinner targets' spectra are flatter, while the thicker-target spectra seem to slope

downward with increasing photon energy. This "sloping" is presumed to be due to the secondary-processes (which manifest themselves at lower energies) that are known to contribute to the thick-film spectra.

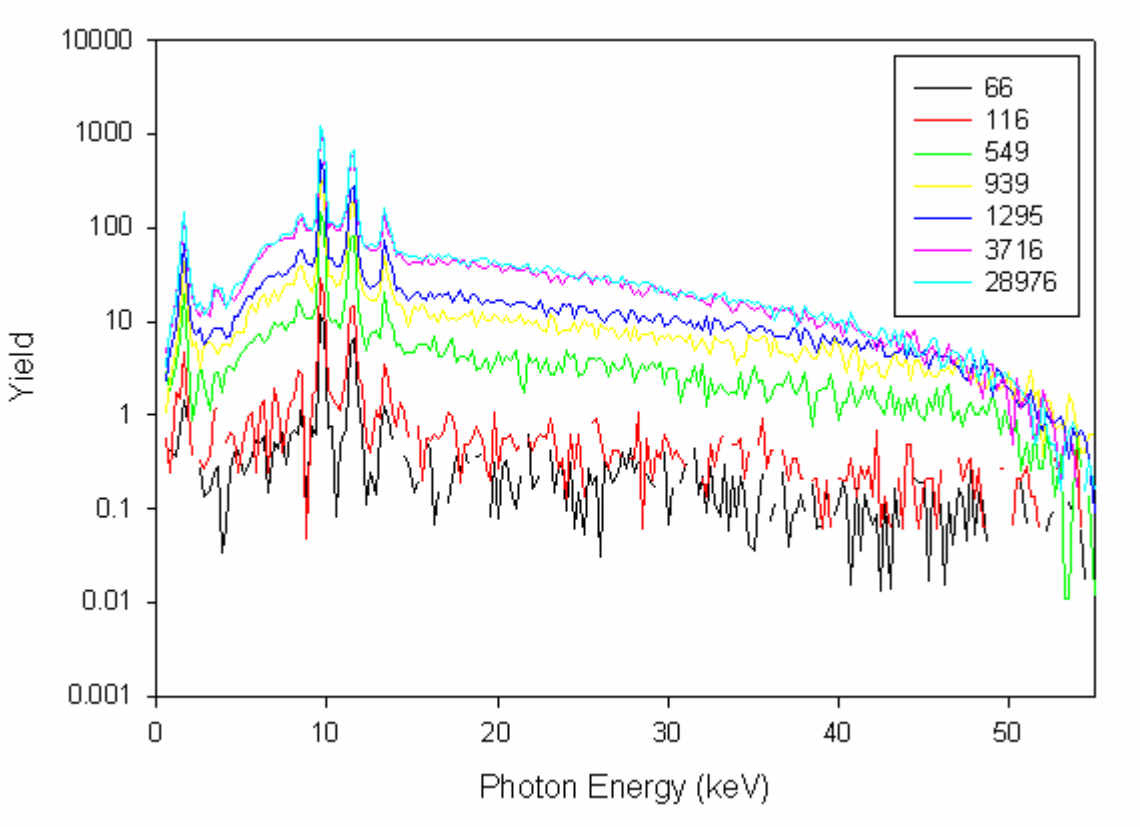

Figure 4 Plot of the 135 degree yields (in photons per steradian per keV) as a function of photon energy for all seven targets used in the experiments (thicknesses given in $\mu g/cm^2$)

It's also of note that the yields for the two thickest films (3716 and 28976 $\mu g/cm^2$) are almost identical throughout the energy range. This demonstrates the point that – beyond a certain target-thickness - the amount of bremsstrahlung radiation produced is relatively insensitive to the target film's thickness. In this case, both targets seem to have reached this "saturation" point, and the yield seems to be independent of target-thickness beyond this point. This apparent saturation is due to the fact that the energy of the

electrons that penetrate deep into the thicker targets is low enough that most of the photons produced as a result are absorbed in the target.

It can also be observed that, very near the (53 keV) kinematic end-point, the yields also seem to be less dependent on target-thickness. This is presumed to be due to the fact that photons at the higher energies are produced when the electron first enters the target (i.e. at relatively "shallow" parts of the target), before the electron has lost a significant portion of its energy. This explains why the spectra for the thicker targets have broader end-points, while the spectra for the thinner targets exhibit sharper end-points.

4.2 Yields as a Function of Target-Thickness

Figure 5 is a plot of the 25, 35, and 45 keV yields as a function of (logarithmic) target thickness (in $\mu g/cm^2$). The 5 and 10 keV yields weren't included because of the difficulty in dealing with the gold x-ray peaks at 9.7, 11.4, and 13.4 keV. The yield values were obtained by summing the yields over a 10 keV energy range, and plotting the value at the average energy. For example, the 45 keV plot was generated by summing the yield for each target from 40 to 50 keV, and plotting the yield value against the measured thickness of the corresponding target.

The figure demonstrates several things. Firstly, it gives us some idea of at what thickness a film first starts to exhibit thick-film behavior. As demonstrated especially well in the 25 keV plot, the yield increases dramatically starting at a thickness of around 1000 $\mu g/cm^2$. This indicates that while films such as the 549 $\mu g/cm^2$ gold target cannot be considered to be purely "thin", they cannot yet be considered "thick" either (i.e. dominated by secondary-process bremsstrahlung).

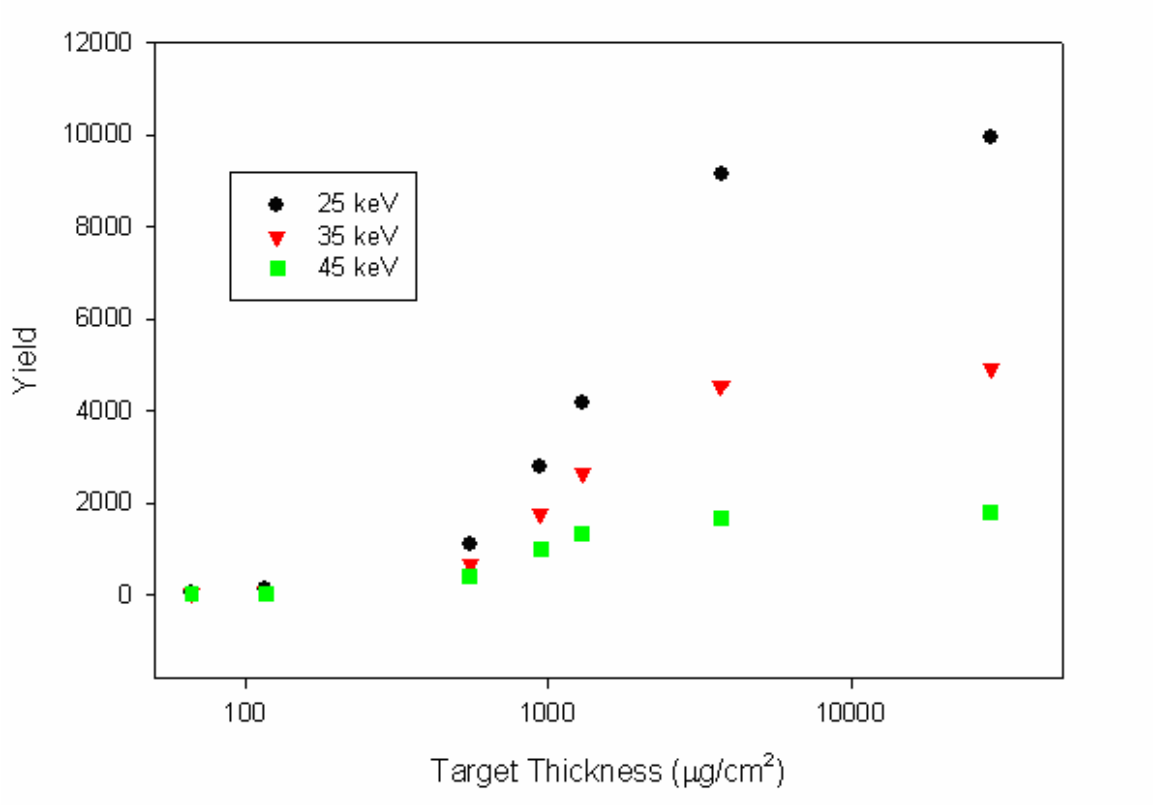

Figure 5 Plot of the 25, 35, and 45 keV yields as a function of target-thickness (135 degree data)

Secondly, a comparison of the 25, 35, and 45 keV plots demonstrates what was mentioned earlier: that the yield is less dependent on target thickness at higher energies due to the fact that the high-energy bremsstrahlung photons are produced at relatively "shallow" parts of the targets. The figure clearly shows that the 45 keV plot is much more "flat" than the 25 keV plot, or even the 35 keV plot.

Finally, all three plots level-off after they reach the aforementioned "saturation point". This provides further indication that, after a certain target-thickness value, the bremsstrahlung radiation yield becomes independent of the any additional thickness. This "saturation point" seems to be somewhere around a thickness of 2000 $\mu g/cm^2$.

4.3 135 Degree Ratio Comparisons

Figures 6 through 10 are ratio comparisons of the experimental and PENELOPE-generated data. As before, the experimental data has been normalized according to the charge collected, while the PENELOPE data has been normalized according to the number of "events". The amount of charge collected need not be related to the number of events (other than to achieve satisfactory statistics) due to the fact that taking ratios "cancels out" these factors (as well as other factors such as detector efficiency).

The experimental data was taken with the Ge detector using a solid angle of 1.62e-4 steradians, centered at 135 degrees. The PENELOPE data, on the other hand, was summed from 130 to 140 degrees. As stated earlier in this paper, our previous studies have involved comparing experimental data with PENELOPE-generated data summed from 0 to 180 degrees, but we've since corrected this problem, which is important when taking into consideration the fact that bremsstrahlung is angle-dependent. Our purpose behind the comparisons is to try and discern whether or not there is any polarizational bremsstrahlung contribution for solid film targets by noting any deviations from the (normal bremsstrahlung) PENELOPE ratios. We would typically expect a polarizational bremsstrahlung contribution to manifest itself as a ratio discrepancy in the lower-energy region of the spectrum, where polarizational contributions have been seen previously [Portillo et al., 2003].

A comparison of the experimental ratio of the 116 $\mu g/cm^2$ and 66 $\mu g/cm^2$ target yields to the corresponding PENELOPE-generated ratio can be seen in Figure 6.

Both the shape and the magnitude of the ratios are in good agreement with one another throughout the photon energy range. The shape of both ratios is essentially flat,

indicating that both films can still be considered to be “thin” (i.e. the spectra aren’t dominated by radiation resulting from secondary processes for either of the targets). One might naively expect the ratio to be the same as the ratio of the target thicknesses (~1.76), and this proves to be the case for the ratio of the thinnest two films (but it will soon be shown that this isn’t necessarily the case for thicker targets).The PENELOPE ratio value (averaged over the entire energy range) is 1.66, and the experimental ratio value (also averaged over the entire energy range) is slightly higher at about 1.97. When calculating the average experimental ratio, points in the data with zero values become an issue. This problem was dealt with by averaging over channels until the zero points were eliminated, thus avoiding points in the ratio vs. photon energy plot with infinite or zero values.

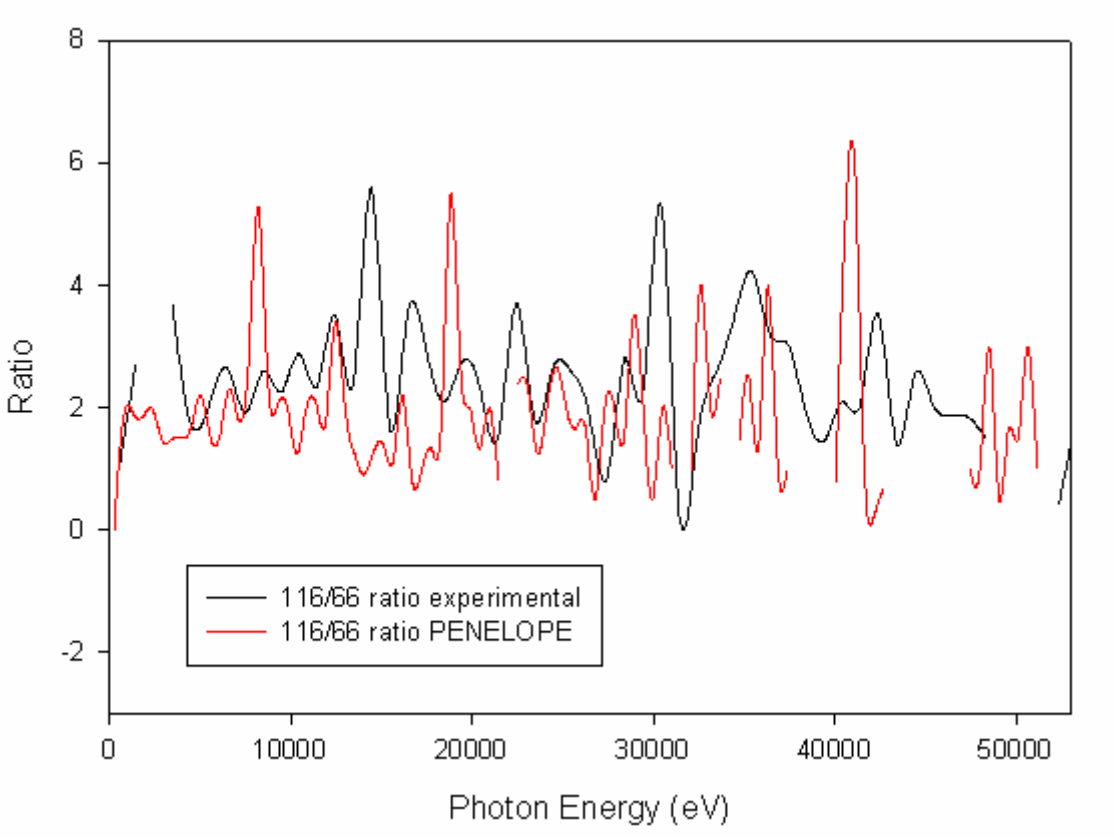

Figure 6 A comparison of the experimental and PENELOPE-generated ratios of the 116/66 μg/cm^2 target yields

It has generally been thought that if there were any polarizational bremsstrahlung contributions to the solid-film spectra, they would be more easily seen in thin-film experiments (such as with the 66 and 116 $\mu g/cm^2$ targets). As previously stated (and soon to be illustrated in cross-section measurements/comparisons) both the 66 $\mu g/cm^2$ and (to a lesser extent) 116 $\mu g/cm^2$ films can safely be consider "thin", in that they seem to follow the single-interaction model. The experimental ratio, when compared to the PENELOPE-generated ratio, doesn't give us any definitive answer as to whether or not there is a polarizational bremsstrahlung contribution (keeping in mind that PENELOPE only simulates normal bremsstrahlung). A comparison of the ratios shows the experimental ratio to be slightly higher over much of the 0 to 10 keV range. This is likely not due to a polarizational contribution, but if it was, it would indicate that the polarizational bremsstrahlung contribution for the 116 $\mu g/cm^2$ target experiment was greater than for the 66 $\mu g/cm^2$ targets experiment, and that the contribution doesn't have the same target thickness-dependence that normal bremsstrahlung has.

Both the experimental and PENELOPE-generated ratios are statistically weaker for the 66 and 116 $\mu g/cm^2$ targets than for the thicker films (although uncertainties for both of the thin films are less than 10%). This accounts for why the ratios are "wavier" and less refined-looking than the comparisons of the thicker films.

A comparison of the experimental ratio of the 28976 $\mu g/cm^2$ and 3716 $\mu g/cm^2$ target yields to the corresponding PENELOPE-generated ratio is shown as a function of photon energy in Figure 7.

As expected, both the shape and the magnitude of the ratios are in good agreement with one another through the entirety of the photon energy range. Both the

experimental and PENELOPE-generated ratios are approximately equal to unity throughout the energy range (the averaged experimental ratio value is 1.11, and the averaged PENELOPE ratio value is 1.09), despite the fact that the ratio of their thicknesses is nearly 7.8. This is in stark contrast to the ratio of the 116 and 66 $\mu g/cm^2$ targets, where the ratio of the radiation yields was approximately equal to the ratio of the target-thicknesses. This is further proof that (beyond a certain target thickness) bremsstrahlung radiation yields for ultra-thick films are independent of the films' thickness. It should also be noted that there doesn't seem to be any sign of the gold x-ray peaks (at approximately 9.7 and 11.4 keV) in the ratios, indicating that they, too, may have a "saturation point".

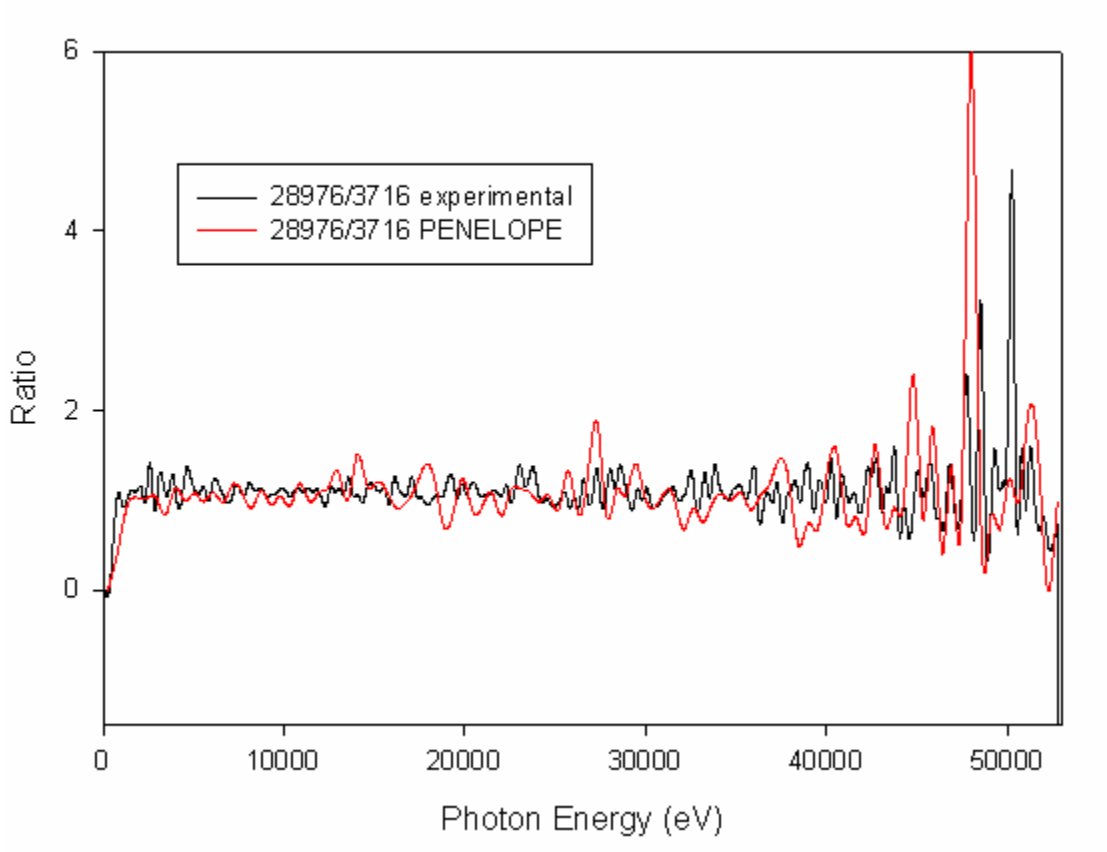

Figure 7 A comparison of the experimental and PENELOPE-generated ratios of the 28976/3716 $\mu g/cm^2$ target yields

Both the PENELOPE-generated and experimental ratios fluctuate more near the higher-energy portion of the spectrum, and this is due to the higher-energy data being statistically weaker than the data at lower energies. It's also interesting that the ratio moves even closer to unity at energies very near the kinematic end-point (~53 keV), demonstrating an earlier point that yields near the end-point are independent of the target films' thickness.

The experimental ratio of the 3716 μg/cm^2 and 1295 μg/cm^2 target yields is compared to the PENELOPE-generated ratio for the same target thicknesses in Figure 8 (as a function of photon energy).

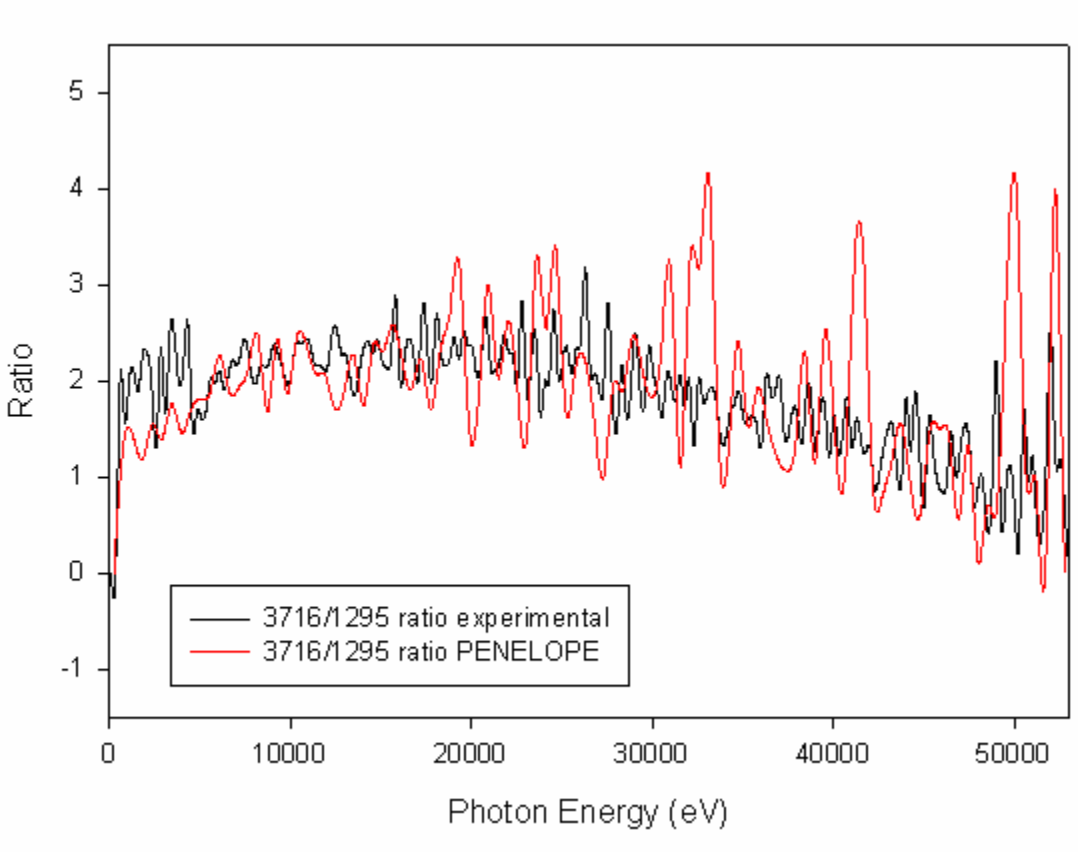

Figure 8 A comparison of the experimental and PENELOPE-generated ratios of the 3716/1295 μg/cm^2 target yields

The plots agree in both shape and magnitude throughout most of the photon energy range (there is some discrepancy at energies below 5 keV), and both ratios approach unity as the photon energy approaches 53 keV. As noted previously, this is because higher-energy radiation (near the initial energy of the incident electron) is a result of electron-atom interactions near the surface of the target film, and is thus less dependent (virtually independent) on the target's thickness. Lower-energy radiation, on the other hand, is the result of interactions deeper within the target film, and is therefore more dependent on the target's thickness. Radiation that originates from areas other than the surface is also susceptible to energy loss due to x-ray absorption.

This ratio comparison is an interesting one, because this one has a much more curved shape than the previous two that we've reviewed (which were both relatively flat). It's also interesting because it's a case where we're comparing a target for which secondary-processes (where a single incident electron interacts with multiple target-atoms) are significant to a slightly thinner target (1295 $\mu g/cm^2$) where – despite the fact that this film certainly couldn't be considered to be "thin" (following a single-interaction model) – it's not quite thick enough to be considered an "ultra-thick" film (where secondary-processes are significant and virtually all of the incident electrons are stopped by the target). Unlike the first ratio that we looked at (Figure 6), the yield ratio can't be approximated by the ratio of thicknesses; but unlike the last ratio that we looked at (Figure 7), the yield ratio isn't equal to unity throughout the energy range, indicating that the 1295 $\mu g/cm^2$ film probably is still in the realm where the yield is still somewhat dependent on the target's thickness.

The experimental ratio is significantly higher than the PENELOPE ratio below 5 keV for reasons that are not yet fully understood. It is likely due to the fact that the thicker target produces more radiation as a result of M-shell characteristic x-rays (of energies in the 0 to 10 keV range), and this M-shell radiation is not reproduced by PENELOPE, as previously noted.

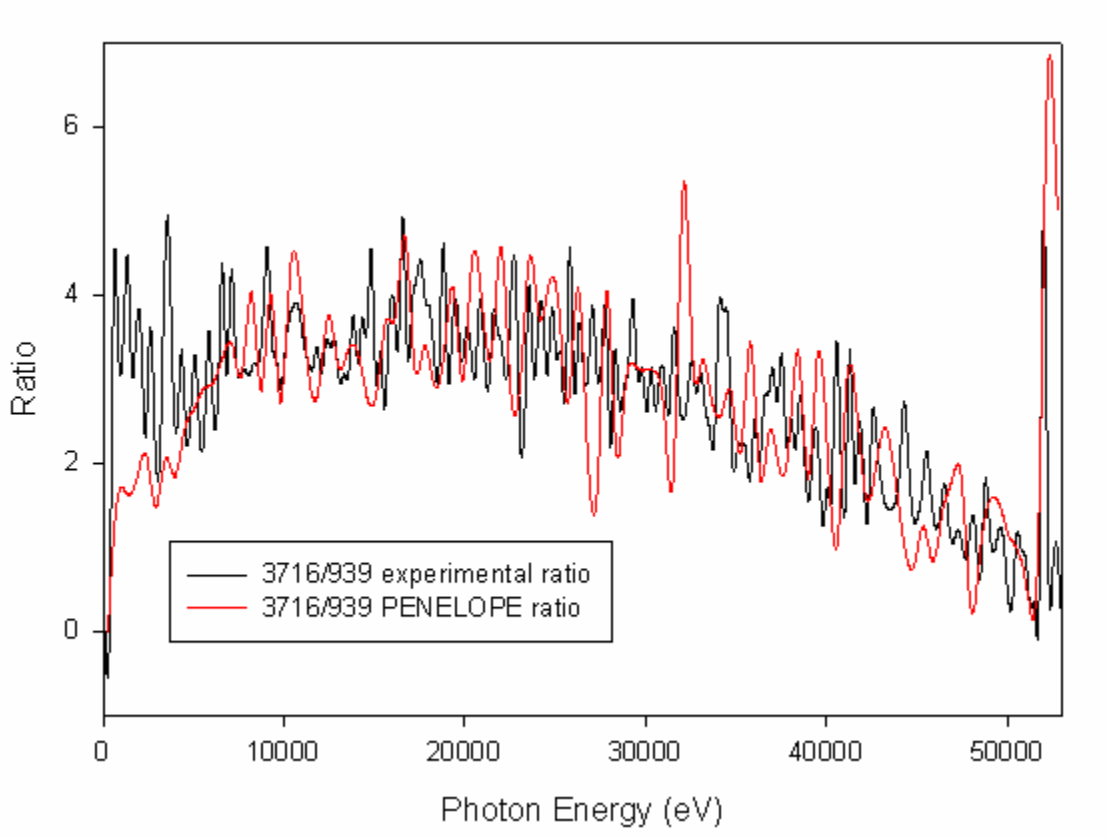

Figure 9 A comparison of the experimental and PENELOPE-generated ratios of the 3716/939 μg/cm^2 target yields

Like the 3716 μg/cm^2 to 1295 μg/cm^2 film ratio, the ratio of the radiation yield for the 3716 μg/cm^2 target to the yield for the 939 μg/cm^2 target (the comparison can be seen in Figure 9) is curved and approaches unity at higher energies. The PENELOPE-generated ratio is in excellent agreement with the ratio of the experimental data in both

shape and magnitude, with the exception of a slight difference at energies less than 5 keV (as with the previous comparison). In this range, just as with the 3716/1295 ratio, the experimental data ratio is slightly higher than the PENELOPE-generated ratio. As before, we think that it is likely due to the fact that PENELOPE doesn't reproduce M-shell characteristic x-rays. This ratio comparison, like the last one, compares a target for which secondary-processes are significant (the 3716 μg/cm^2 target) to a thinner target (although not considered to be truly "thin") where secondary-processes are less dominant.

A comparison of the experimental ratio of the 549 μg/cm^2 and 116 μg/cm^2 target bremsstrahlung yields to the corresponding PENELOPE-generated ratio can be seen in Figure 10.

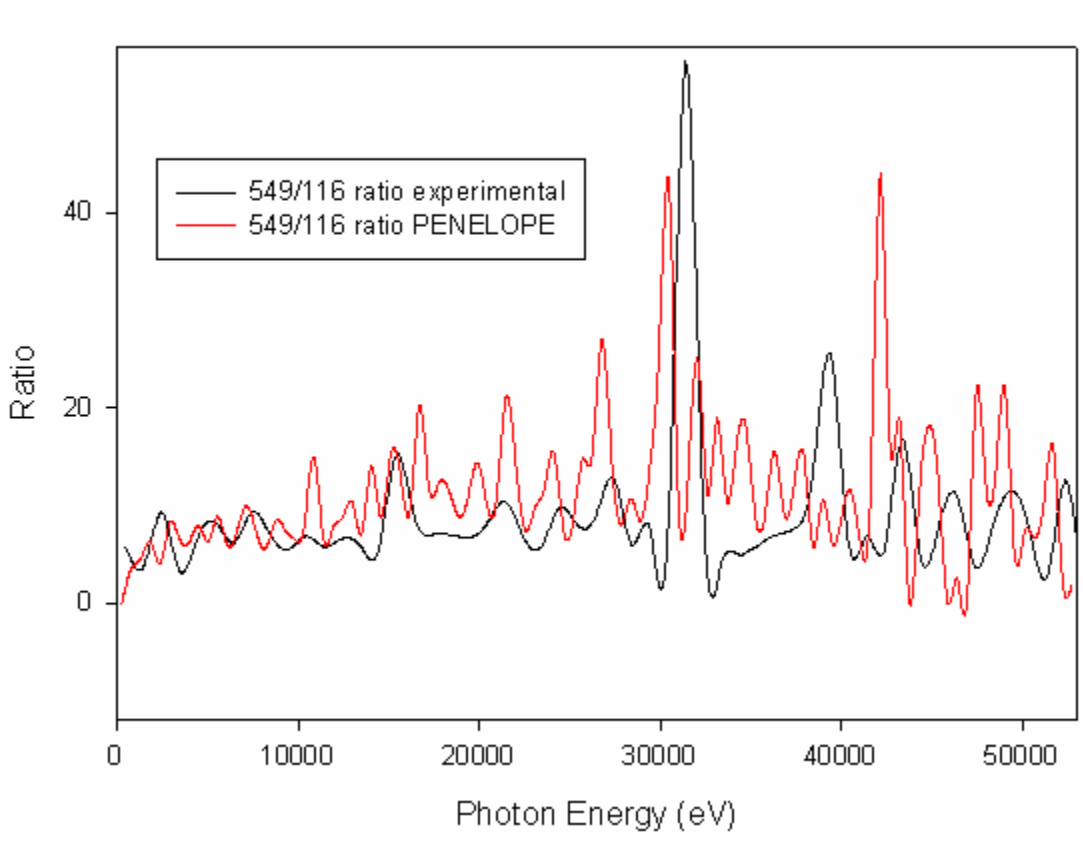

Figure 10 A comparison of the experimental and PENELOPE-generated ratios of the 549/116 μg/cm^2 target yields

The shapes of the two ratios are in relatively good agreement with one another, but the magnitude of the ratio of the experimental data seems to be slightly lower than the PENELOPE-generated ratio. This is possibly due to the pin hole in the 549 $\mu g/cm^2$ target (see Appendix B for details), which would yield slightly less radiation than if there were no hole at all, thus lowering the 549/116 ratio value slightly. The ratio value for the experimental data (averaged over the entire photon energy range) is equal to 8.8, while the (also averaged) ratio of the PENELOPE-generated data is slightly higher at 11.3.

This ratio is an interesting one (and it's disappointing that the pin hole seems to have affected the results) because it compares a truly "thin" target (the 116 $\mu g/cm^2$ film) with a target where secondary-processes may have begun to contribute to the radiation yield (the 549 $\mu g/cm^2$ film). The difference in the magnitudes of the ratios makes it difficult to glean any hints about possible polarizational bremsstrahlung contributions from them.

4.4 135 Degree Data Comparisons

As previously mentioned, ratio comparisons are an attractive way of comparing theoretical and experimental data because factors such as solid angle and efficiency need not be considered (they "cancel out" when taking ratios). When comparing the PENELOPE-generated and experimental data directly, as we do in Figures 11 through 17, we are forced to consider these factors. The efficiency was estimated using experimental efficiency measurements and a best-fit curve (to be discussed in-depth in Appendix C), and the solid angle was carefully measured (using an Am 241 source) and used to calculate the experimental yield. When dealing with both sets of data, the yields were

averaged over a 10 keV energy range (and plotted at the average energy) in order to improve statistics and decrease the amount of error. Only statistical error is represented in the error bars (systematic error will be discussed and estimated in a later section).

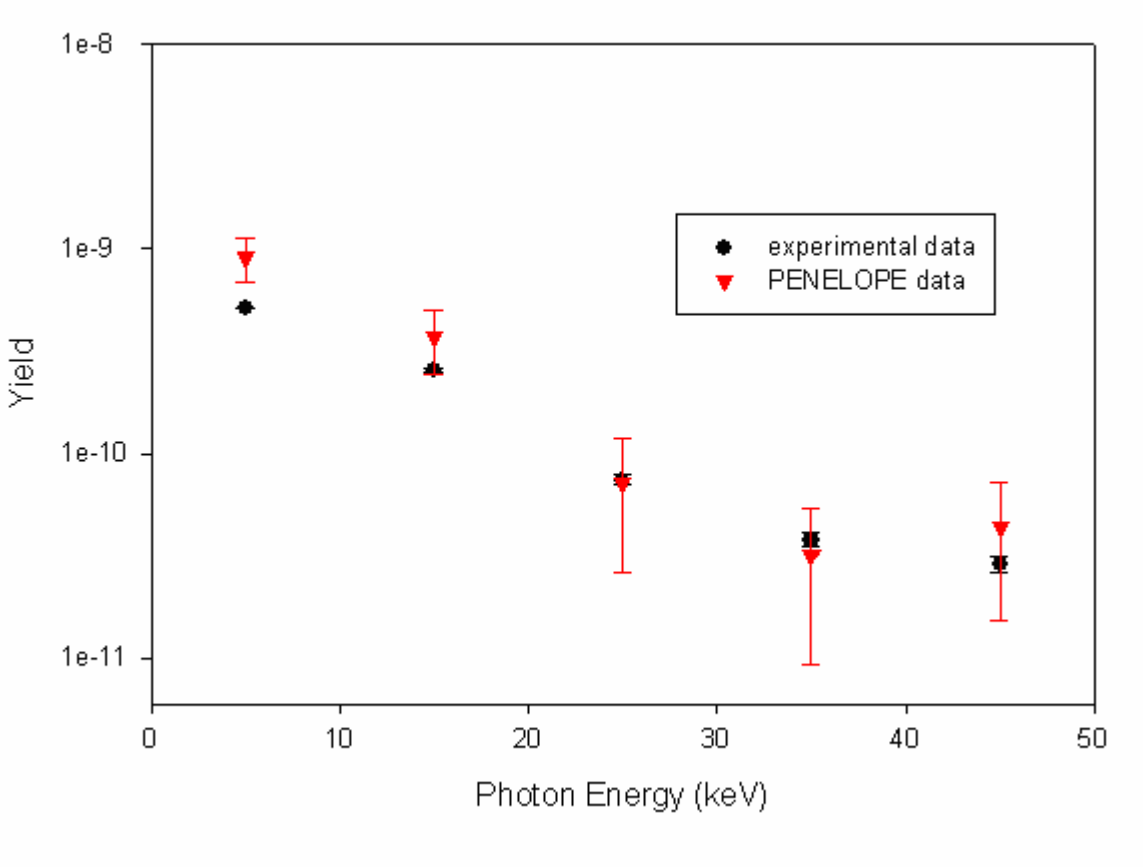

Figure 11 Plot of the experimental and PENELOPE-generated yields (in photons per steradian per keV) for the 66 μg/cm^2 target

Figure 11 is a comparison of the experimental and PENELOPE-generated data (yields as a function of photon energy) for the 66 μg/cm^2 target. The yields are in relatively good agreement with one another, with the exception of a minor discrepancy at 5 keV (where the experimental yield is notably lower). Outside of the point(s) plotted at 5 keV, all of the experimental points lie within the error bars of the PENELOPE data. The PENELOPE data has much more statistical error than the experimental data for all seven targets' data. The exact reason for the discrepancy at 5 keV isn't completely understood,

but one theory is that the Ge detector's efficiency wasn't as good as we estimated in the 0 to 10 keV photon energy range.

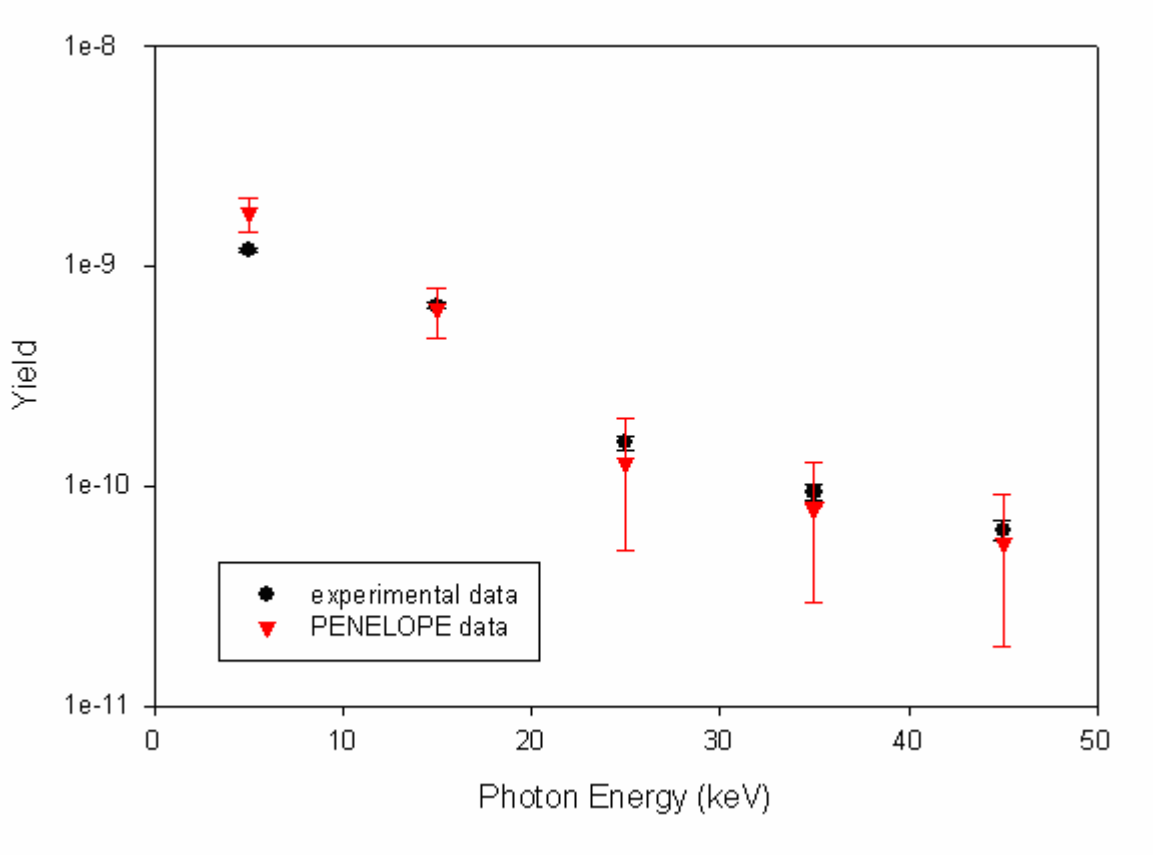

Figure 12 Plot of the experimental and PENELOPE-generated yields for the 116 μg/cm^2 target

Figure 12 is a comparison of the experimental and PENELOPE-generated data for the 116 μg/cm^2 target. As with the 66 μg/cm^2 target, the experimental point at 5 keV is slightly lower than the PENELOPE data at that point. Again, the reason for this may have to do with a bad efficiency estimate, but the exact reason isn't known. At 25, 35, and 45 keV the experimental points seem to be slightly higher than the PENELOPE points, but still well within the error bars. The 15 keV points seem to agree almost exactly.

Plots of the PENELOPE and experimental yields for the 549 μg/cm^2 film are shown in Figure 13. The experimental data is consistently lower than the PENELOPE-generated data throughout the entire energy range, and this is presumed to be due to the fact that the 549 μg/cm^2 film used in the experiments was discovered to have a small hole in it (as has already been mentioned). Despite the error produced by the film's pin-hole for the experimental data, the experimental points at 25, 35, and 45 keV all lie within the error range of the PENELOPE-generated points. As with the previous two data comparisons that we've studied, the experimental data is slightly lower than the PENELOPE data at lower energies (0 to 20 keV); however in this case the hole in the target film may have been a contributing factor.

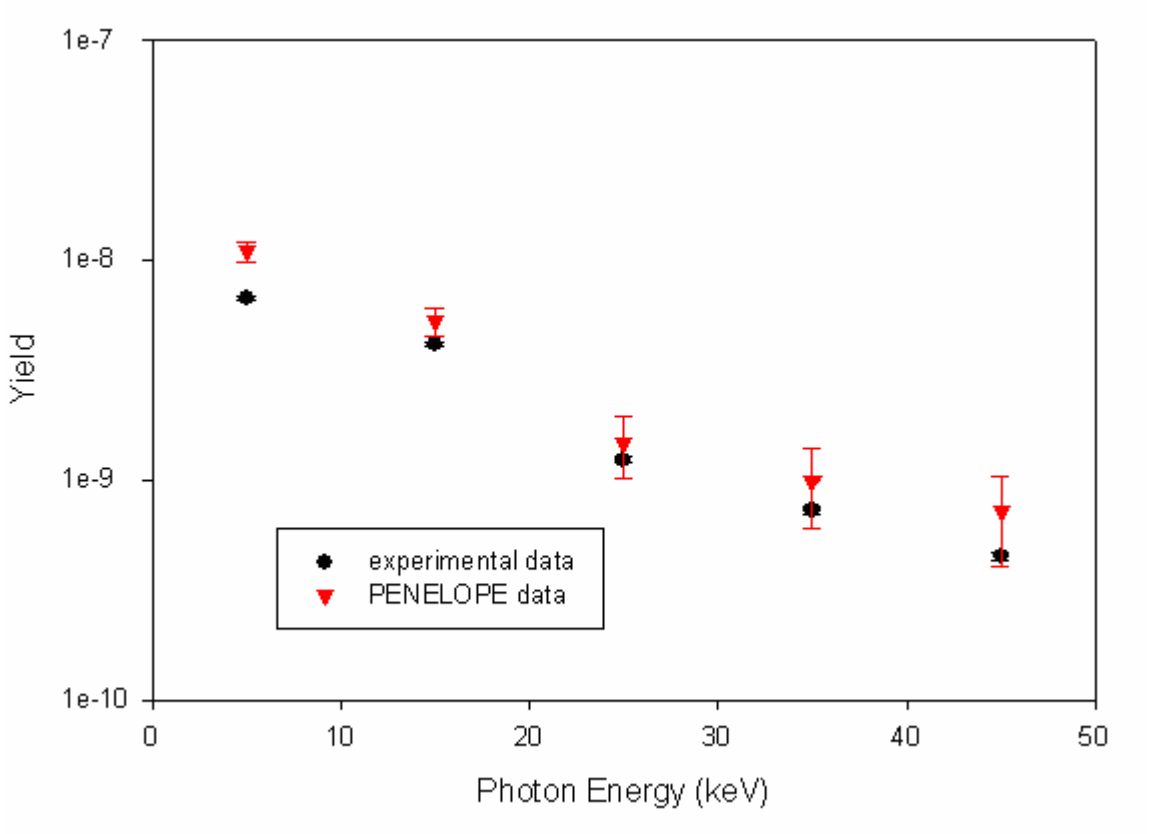

Figure 13 Plot of the experimental and PENELOPE-generated yields for the 549 μg/cm^2 target

Figure 14 is a comparison of the experimental and PENELOPE-generated data for the 939 μg/cm^2 target. It (again) features a discrepancy at 5 keV, with the experimental data being slightly lower than the PENELOPE-generated data. Although each of the other plotted experimental data points are within (or almost within) the error bars of the PENELOPE-generated data points, the experimental yield is consistently (but only slightly) lower than the PENELOPE yield for this particular film.

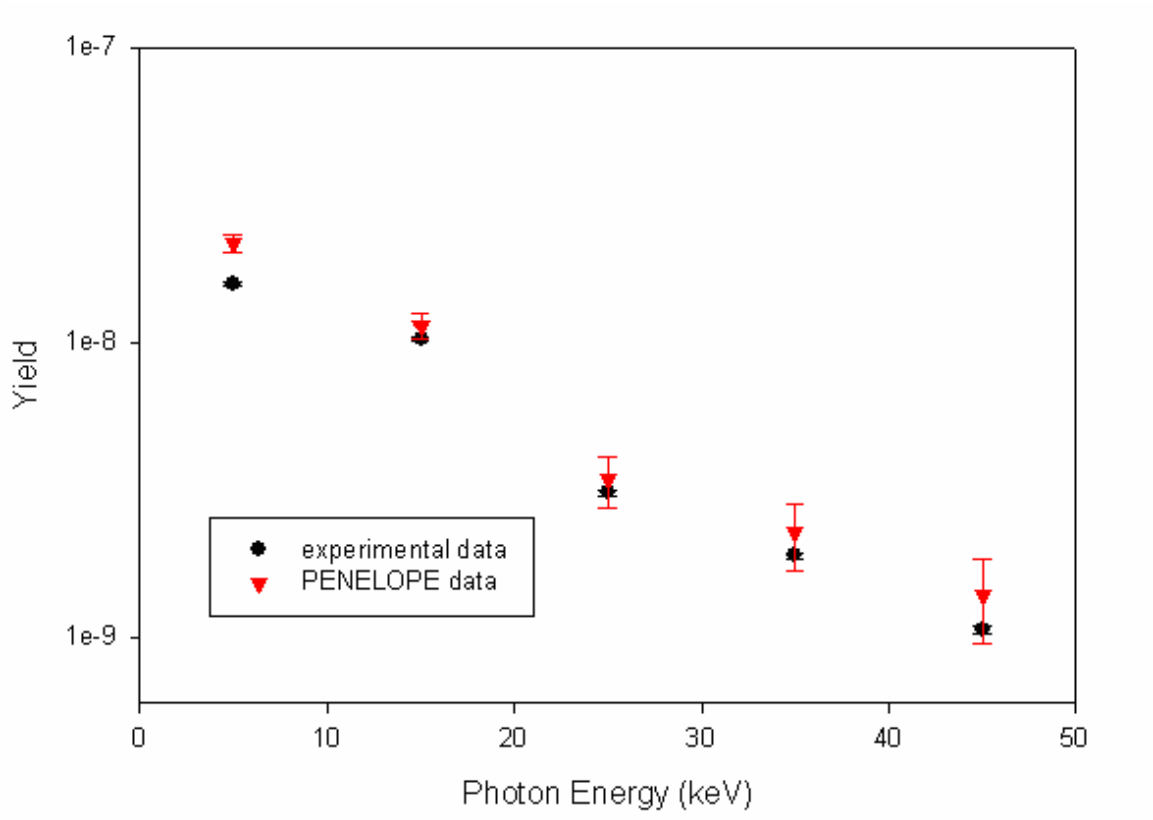

Figure 14 Plot of the experimental and PENELOPE-generated yields for the 939 μg/cm^2 target

The experimental and PENELOPE-generated data for the 1295 μg/cm^2 film (Figure 15) is almost identical to the data for the 939 μg/cm^2 target. The seemingly-

obligatory discrepancy at 5 keV is present, and – despite being within the error bars of the PENELOPE-generated data – the experimental yield is consistently lower than the PENELOPE-generated yield throughout the entire photon energy range.

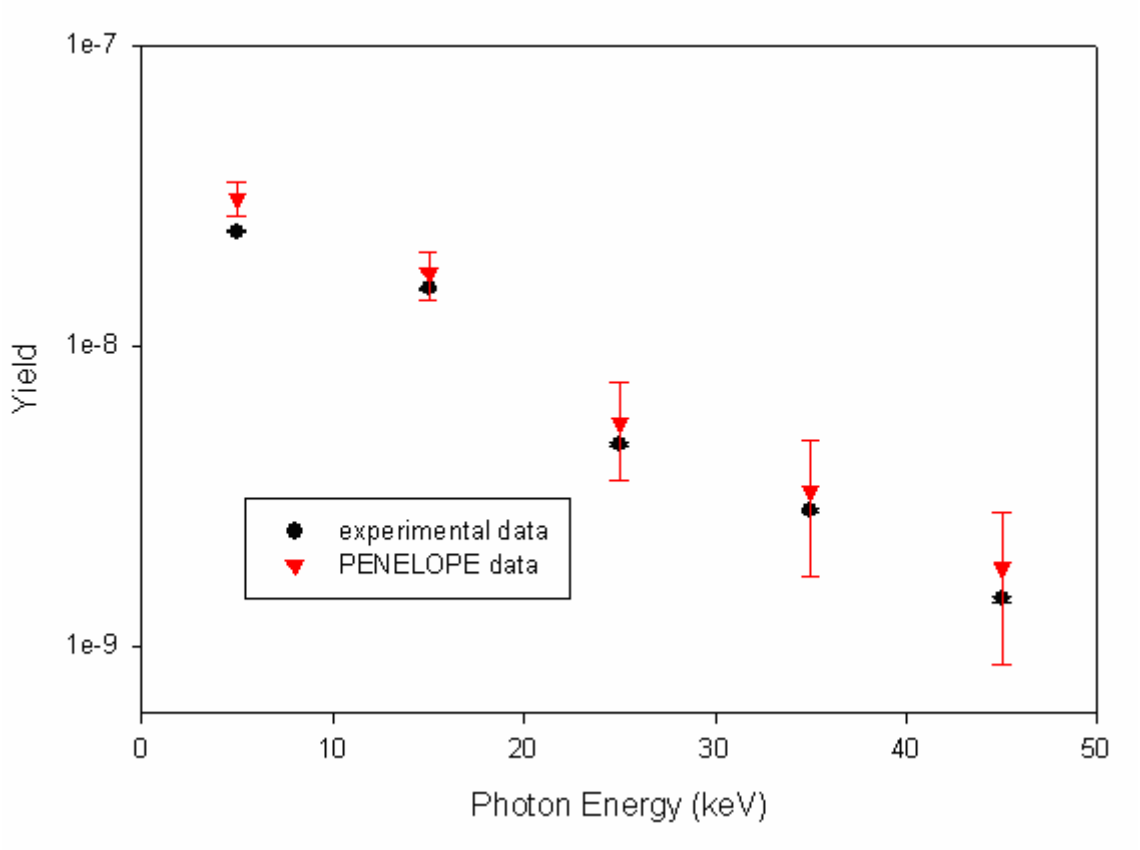

Figure 15 Plot of the experimental and PENELOPE-generated yields for the 1295 μg/cm^2 target

Figure 16 is a comparison of the experimental and PENELOPE-generated data for the 3716 μg/cm^2 target. Although the experimental point at 5 keV is lower than the PENELOPE-data point, it's within the error bar of the PENELOPE data and not nearly as low as in previous cases. Other than that, the experimental yield is in excellent agreement with the PENELOPE-generated yield throughout the photon energy range. But as with

the previous comparisons, the experimental data is consistently lower (albeit it slightly lower) than the simulated data.

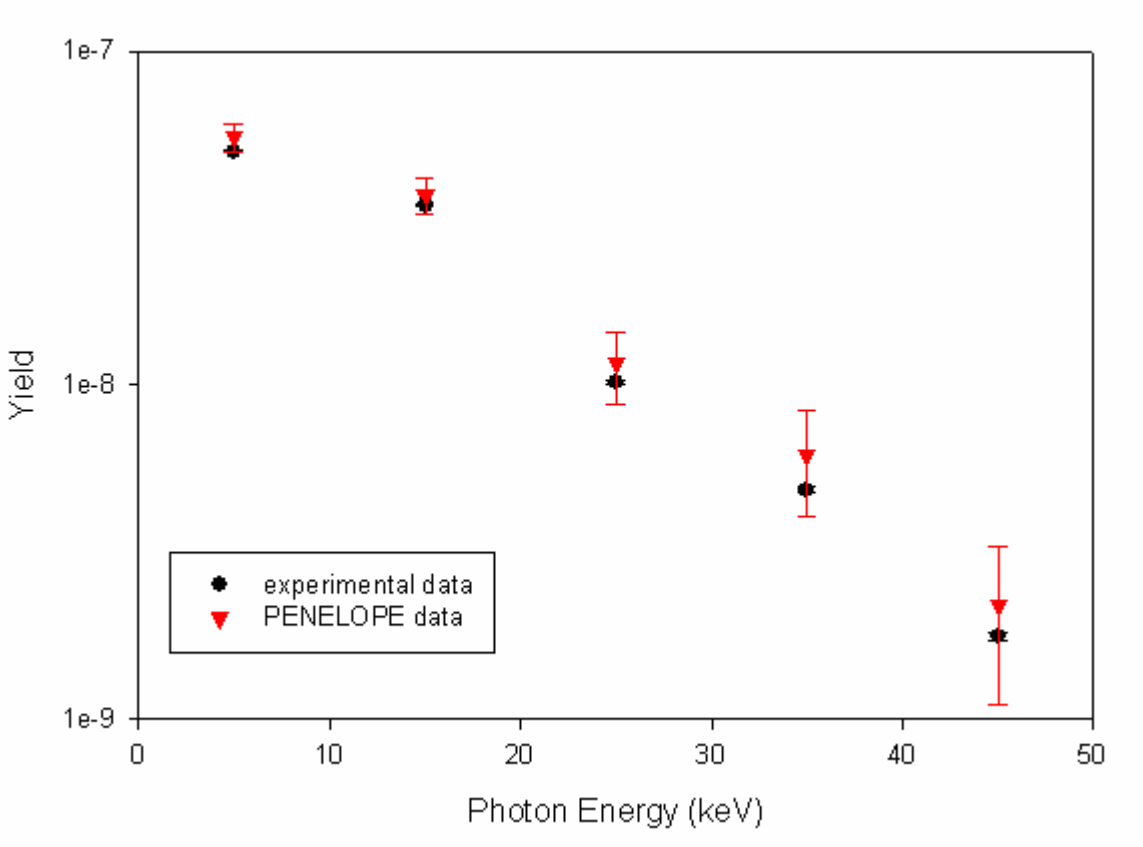

Figure 16 Plot of the experimental and PENELOPE-generated yields for the 3716 μg/cm^2 target

The final comparison of the experimental and PENELOPE-generated yields (for the 28976 μg/cm^2 target) can be seen in Figure 17. Of all the comparisons that we've reviewed thus far, the experimental and PENELOPE-generated yields for this target-thickness seem to agree the best. While (once again) the experimental yield is (very slightly) lower than the PENELOPE yield throughout the entire photon energy range, all five experimental data points are within the uncertainty range of the PENELOPE data. This is somewhat expected, due to the fact that the experimental data for the 28976

μg/cm^2 target features the best statistics, and the fact that both the PENELOPE and the experimental data should feature identical "saturation" yields (note that the 28976 μg/cm^2 target is well beyond the thickness where additional thickness results in an increase in radiation yield).

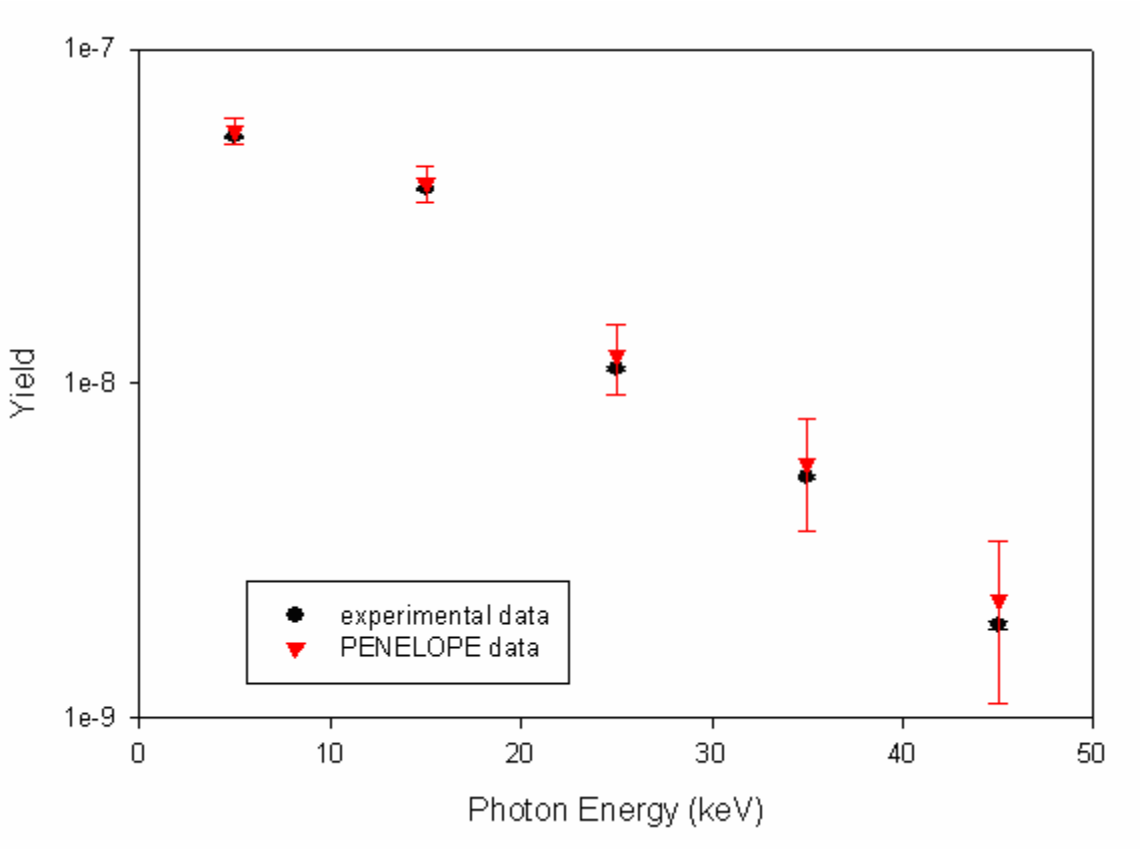

Figure 17 Plot of the experimental and PENELOPE-generated yields for the 28976 μg/cm^2 target

The reason that this comparison features an experimental yield that is slightly lower than the PENELOPE yield (just as with most of the other comparisons) may have something to do with our efficiency estimates (as previously stated) being little off. However (and more importantly) the comparisons reveal that our experimental data is consistent with data that has no polarizational bremsstrahlung contribution. If there were

a polarizational bremsstrahlung contribution, we would expect to see experimental yields that were higher than the yields generated by PENELOPE, rather than lower.

4.5 135 Degree Cross-Section Measurements

A plot of the absolute doubly-differential cross-section measurements (for the 66 and 116 $\mu g/cm^2$ targets) as a function the energy of the photons produced in the experiments can be seen in Figure 18. The figure also includes theoretical predictions for both normal bremsstrahlung and the stripping approximation (where a polarizational bremsstrahlung contribution is included) for an infinitely thin gold film. The doubly-differential cross-section for solid targets is defined as:

$$(d^2\sigma/dkd\Omega) = (\beta^2/Z^2)\,[(k_{average}\,N(k))/(\tau\,\Delta k\,a(k)\,\Delta\Omega\,\varepsilon(k)\,N_e)]$$

where N(k) is the number of counts at photon energy k, N_e is the number of incident electrons, τ is the target's thickness in atoms/cm^2, $\Delta\Omega$ is the solid angle subtended from the target to the detector, $\varepsilon(k)$ is the detector-efficiency (to be discussed in-depth later), a(k) is the absorption of the scattered electron absorber, Z is the Z-value of the target-material (79, for gold), $k_{average}$ is the average energy value of the energy region of interest, and β is the velocity of the incident electrons divided by the speed of light in a vacuum.

The doubly-differential cross-section values and the corresponding uncertainties are shown in Chart 2. The uncertainties shown are all purely statistical.

Cross-section measurements are given for both targets at energies of 25, 35, and 45 keV, along with a fourth (estimated) point at 15 keV. The 15 keV point was measured using only an estimate of the bremsstrahlung produced at this energy, due to the fact that the x-ray peaks at 11.4 and 13.4 keV had to be taken into account. This was done by

visually estimating the curve of the continuous spectra from 10 to 20 keV, and substituting in the estimated yield for the portions affected by the gold x-ray peaks. For each of the points in the figure, the bremsstrahlung radiation yield was summed over a 10 keV range, and plotted at the energy average of that range.

target thickness ($\mu g/cm^2$)	energy (keV)	DDCS measurement (mB/sr)	stat. uncertainty (mB/sr)	total uncertainty (mB/sr)
66	15	0.252	0.011 (4.6%)	0.016 (6.3%)
66	25	0.251	0.014 (5.6%)	0.018 (7.0%)
66	35	0.178	0.014 (7.7%)	0.016 (8.8%)
66	45	0.176	0.015 (8.7%)	0.017 (9.7%)
116	15	0.440	0.019 (4.3%)	0.026 (6.0%)
116	25	0.299	0.019 (6.4%)	0.023 (7.7%)
116	35	0.251	0.020 (8.1%)	0.023 (9.1%)
116	45	0.217	0.021 (9.8%)	0.023 (10.7%)

Chart 2 135 degree doubly-differential cross-section measurements and the corresponding uncertainties (both statistical and total) for the two thinnest targets

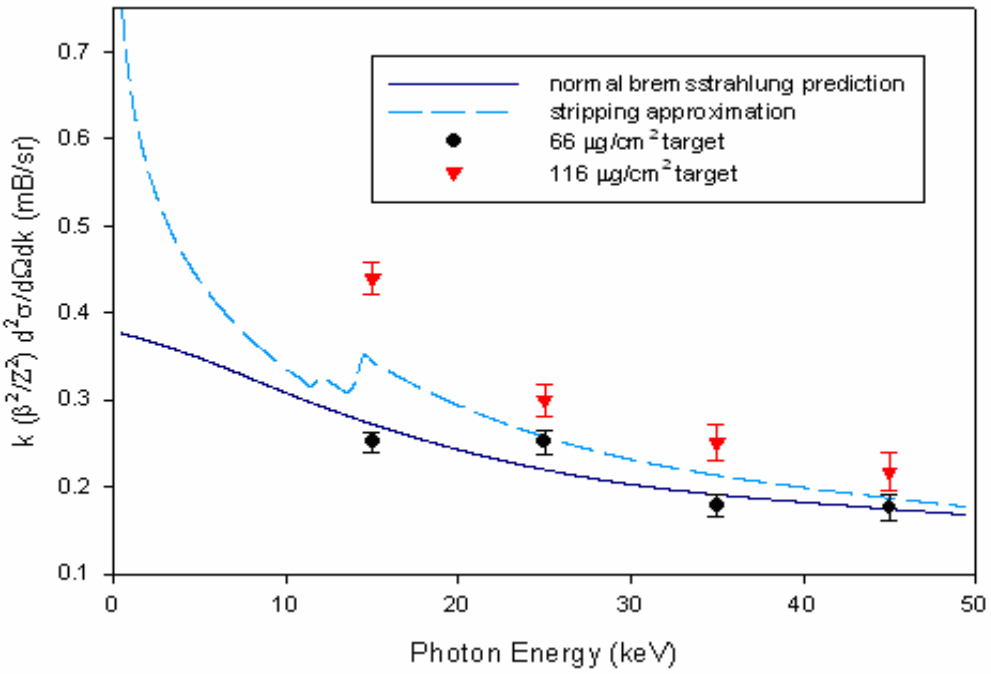

Figure 18 135 degree cross-section measurements as a function of photon energy for the 66 and 116 $\mu g/cm^2$ targets compared with the stripping approximation and normal bremsstrahlung predictions for an infinitely thin target

The 66 μg/cm^2 target cross-sections are in extremely good agreement with the (normal bremsstrahlung) theory, but are well below the stripping approximation for thin films.

The comparison with theory indicates no polarizational bremsstrahlung contribution to the 66 μg/cm^2 film data, and suggests that the single-interaction model is adequate for films near this thickness. With the exception of the point at 25 keV, all of the points are very close to the predicted normal bremsstrahlung cross-section.

The 116 μg/cm^2 target cross-sections are higher than both the normal bremsstrahlung prediction and the stripping approximation (keep in mind, that both are purely “thin” film predictions).

The comparison with theory indicates that the 116 μg/cm^2 target may already be thick enough that the single-interaction model is no longer adequate. While the slope of the points is similar to the slope of the plotted points for the 66 μg/cm^2 target (except at the estimated 15 keV point), the cross-section is significantly greater throughout the entire photon energy range.

V. 90 degree results

5. 1 Notes On The Experiments and PENELOPE

The experimental data obtained for bremsstrahlung radiation at an angle of 90 degrees from the electron beam-line employed the chamber set-up shown in Figure 19.

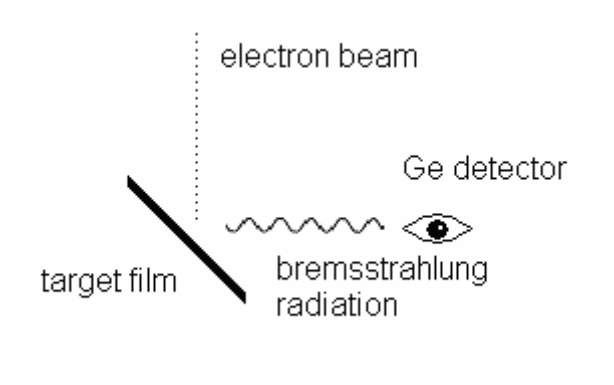

Figure 19 Diagram of the 90 degree geometry used in the experiments

Notice that the target film was positioned at an angle of 45 degrees in relation to both the beam-line, and the Ge detector; this results in the effective target-thickness being a factor of 1.41 (the secant of 45 degrees) thicker than the targets' measured thicknesses. For example, our 66 $\mu g/cm^2$ gold film now has an effective thickness of 94 $\mu g/cm^2$. Unfortunately, this feature of our 90 degree set-up prevents us from directly comparing our 135 and 90 degree data, due to the fact that the data sets are for targets of different effective thicknesses.

Another issue revealed itself when we attempted to compare our experimental data taken at 90 degrees with the PENELOPE-generated data for 90 degrees. The PENELOPE program provides simulated data for an experimental set-up as shown in Figure 20. Unlike our experimental schematic (Figure 19), where the target is at an angle of 45 degrees from both the beam-line and the detector, the PENELOPE program

simulates bremsstrahlung for a target that is positioned normal to the beam-line, and parallel to the solid angle subtended at the detector by the target's interaction region.

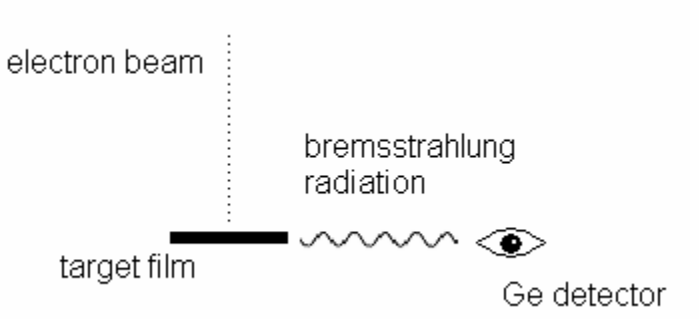

Figure 20 Diagram of the 90 degree geometry simulated by PENELOPE

The problem is that PENELOPE (correctly) accounts for bremsstrahlung radiation that is absorbed by the target, itself; and due to the fact that the target (in the simulation) is positioned at 0 degrees from the detector, this absorption becomes significant, especially when dealing with thicker films. The experimental set-up, on the other hand, has the target situated at an angle of 45 degrees from the detector, and thus it isn't as susceptible to absorption issues. This problem was first encountered when studying the PENELOPE-generated data for angles near 90 degrees. It was realized that, due to this absorption issue, PENELOPE was predicting that the radiation would actually decrease as the target-thickness increased for the thicker films. When studying the PENELOPE data for thin-film situations, this phenomenon wasn't observed. As might be expected, the absorption issue affected the lower-energy portions of the spectra more than the higher-energy portions (where most of the radiation is a result of electron-atom interactions near the film's surface). Due to this unexpected issue, the comparisons with the PENELOPE-generated data (and ratios) aren't as accurate as with the 135 degree data.

5.2 Spectra

Figure 21 is a plot of the radiation yields obtained using each of the targets (detected at an angle of 90 degrees in relation to the electron-beam) as a function of photon energy. As with the data collected at 135 degrees, the incident electrons' energy was approximately 53 keV for all of the experiments.

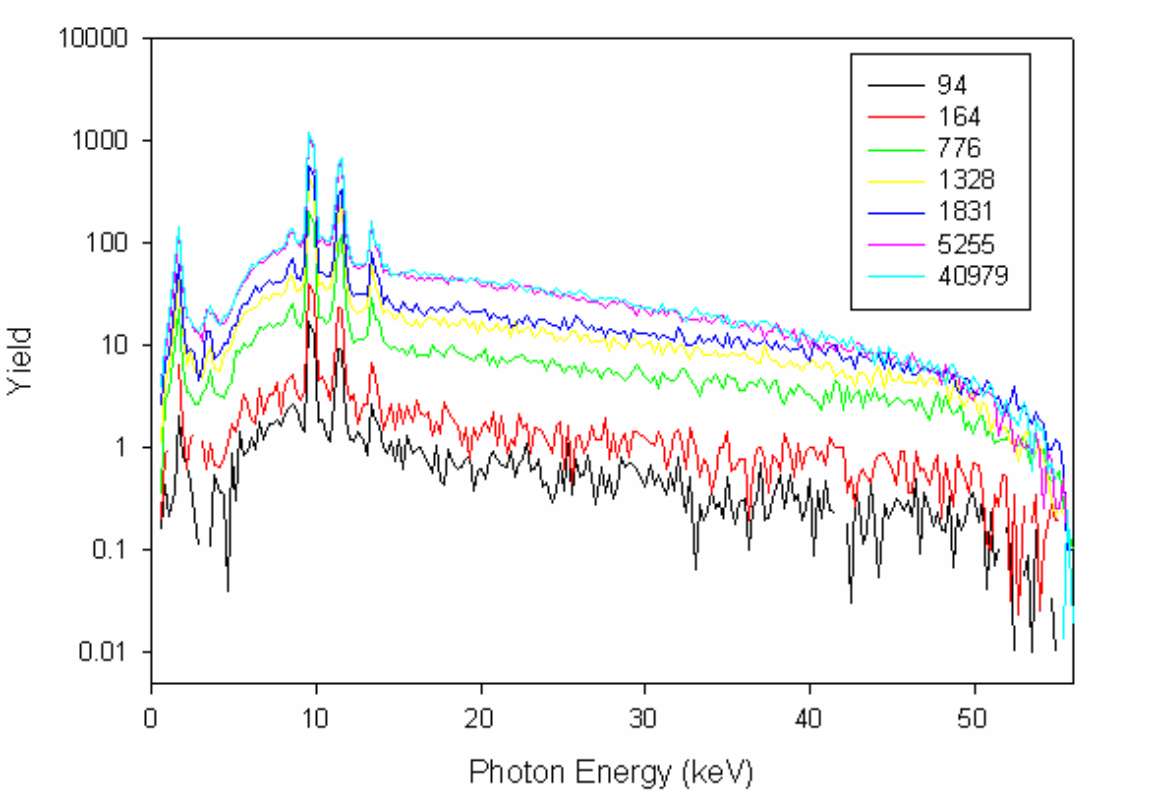

Figure 21 Plot of the 90 degree yields as a function of photon energy for all seven targets used in the experiments (thicknesses given in μg/cm^2)

As with the spectra for the data obtained at 135 degrees, the data (normalized according to charge-collection) for the thinner films (specifically, the 66 and 116 μg/cm^2 targets) isn't as statistically strong as the data for the other films, making the plots look a little more "rough" than the thick-film plots.

The 90 degree data is similar to the data taken at 135 degrees in other ways, as well. Just as with the 135 degree data, we can see that the thinner targets' spectra are relatively flat, while the thicker-target spectra seem to slope downward with increasing photon energy (remember: this "sloping" is presumed to be due to the secondary-processes that are known to contribute to the thick-film spectra); and once again, the yields for the two thickest films (5255 and 40979 $\mu g/cm^2$) are almost identical throughout the energy range. As we've seen previously, the yields also seem to be less dependent on target-thickness in the photon energy region very near the (53 keV) kinematic end-point.

The only obvious difference between the spectra of the 90 and 135 degree data is that the 90 degree yields (for the thinner films) are higher than the 135 degree yields by a factor of approximately two. The yields for the thicker films, on the other hand, seem to be almost identical to one another. This difference (in the thin-film data) demonstrates the angle-dependence of bremsstrahlung.

5.3 Yields as a Function of Target-Thickness

Figure 22 is a plot of the 25, 35, and 45 keV yields as a function of (logarithmic) target thickness (in $\mu g/cm^2$). The 5 and 10 keV yields weren't included (as with the 135 degree data) because of the difficulty in dealing with the gold x-ray peaks at 9.7, 11.4, and 13.4 keV. The yield values were obtained by summing the yields over a 10 keV energy range, and plotting the value at the average energy.

The plot is very similar to Figure 5 (for the 135 degree data). Again, we can see that somewhere around 1000 $\mu g/cm^2$, the yield increases dramatically; indicating that -

beyond this approximate thickness – thick-target bremsstrahlung starts to dominate the radiation yield.

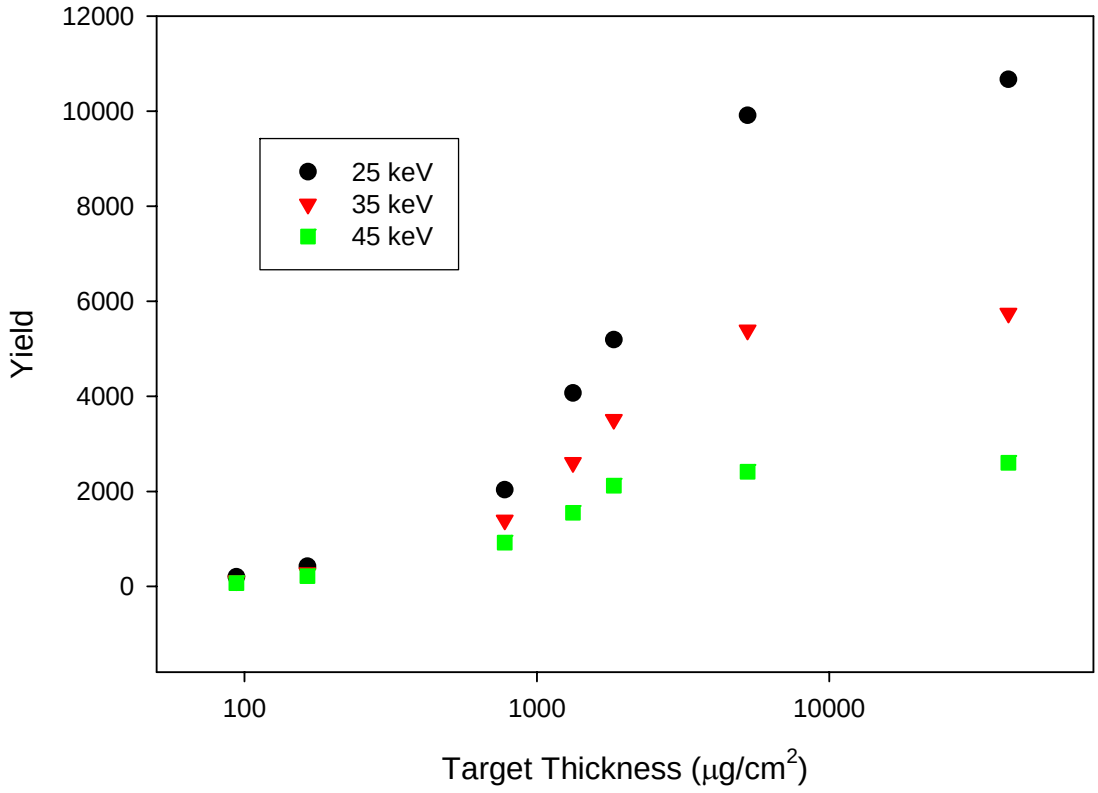

Figure 22 Plot of the 25, 35, and 45 keV yields as a function of target-thickness (90 degree data)

We also can see that somewhere around 2000 μg/cm^2 all three plots start to level-off, once again indicating a "saturation" point.

5.4 90 Degree Ratio Comparisons

Figures 23 through 25 are ratio comparisons of the experimental and PENELOPE-generated data. The first two are comparisons of thin/thin film ratios (where the aforementioned issue with the PENELOPE simulations is less of a problem), and the

third is a thick/thick film comparison that is included to serve as an example of exactly how this PENELOPE issue affects the data. As with the 135 degree ratio comparisons, the experimental data has been normalized according to the charge collected, while the PENELOPE data has been normalized according to the number of "events". The experimental data was taken with the Ge detector using a solid angle of 1.16e-4 steradians, centered at 90 degrees. He PENELOPE data, on the other hand, was summed from 85 to 95 degrees.

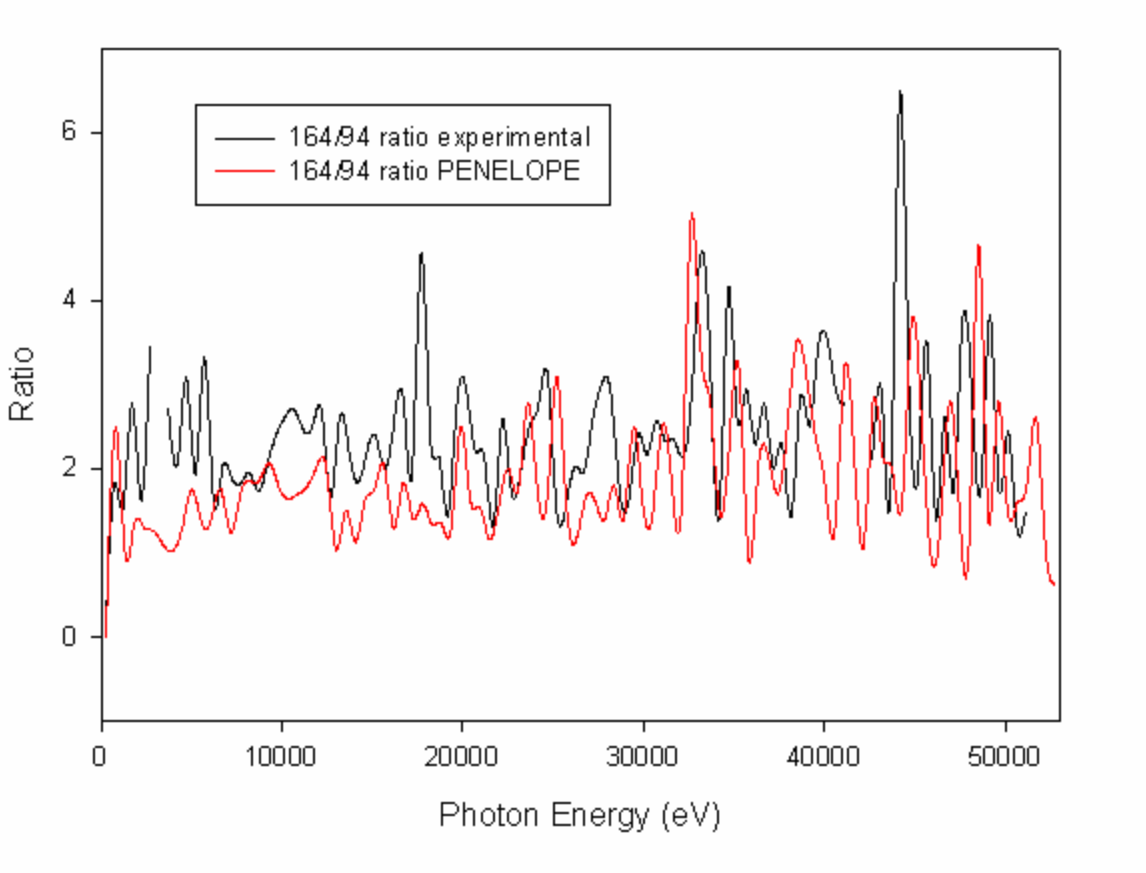

Figure 23 A comparison of the experimental and PENELOPE-generated ratios of the 164/94 μg/cm^2 target yields

A comparison of the experimental ratio of the 164 μg/cm^2 and 94 μg/cm^2 (the effective targets thicknesses of the 116 and 66 μg/cm^2 films at 90 degrees) target yields to

the corresponding PENELOPE-generated ratio can be seen in Figure 23. Both the shape and the magnitude of the ratios are in relatively good agreement with one another throughout the photon energy range. For the most part, the PENELOPE ratio appears to be slightly lower than the experimental data ratio, but the only place where the PENELOPE ratio seems to be significantly lower is in the < 5 keV energy range. The PENELOPE ratio value (averaged over the entire energy range) is 1.86, and the experimental ratio value (also averaged over the entire energy range) is slightly higher at about 2.31. The 22% difference may be due to a variety of factors, including, but not limited to, the radiation absorption issue with the PENELOPE-generated data, weak statistics, and the contribution (to the ratio average) of the aforementioned low-energy discrepancy (possibly due to the fact that PENELOPE doesn't reproduce M-shell radiation). Both the experimental and PENELOPE-generated ratios are statistically weaker for the 94 and 164 $\mu g/cm^2$ targets than for the thicker films, and (similar to its 135 degree counterpart) this accounts for why the ratios are "wavier" and less refined-looking than the comparisons of the thicker films.

A comparison of the experimental ratio of the 776 $\mu g/cm^2$ and 164 $\mu g/cm^2$ (the effective target thicknesses of the 549 and 116 $\mu g/cm^2$ films at 90 degrees) target yields to the corresponding PENELOPE-generated ratio is shown as a function of photon energy in Figure 24. Below about 10 keV, we can see that the ratio of the PENELOPE-generated data is remarkably lower than the ratio of the experimental data. The ratio seems to curve downward (when viewed from right to left) as it approaches 0 keV. This is suspected to be due to the difference between the experimental set-up and the set-up simulated by the

PENELOPE program. Beyond 10 keV, the ratios are in good agreement in both shape and magnitude.

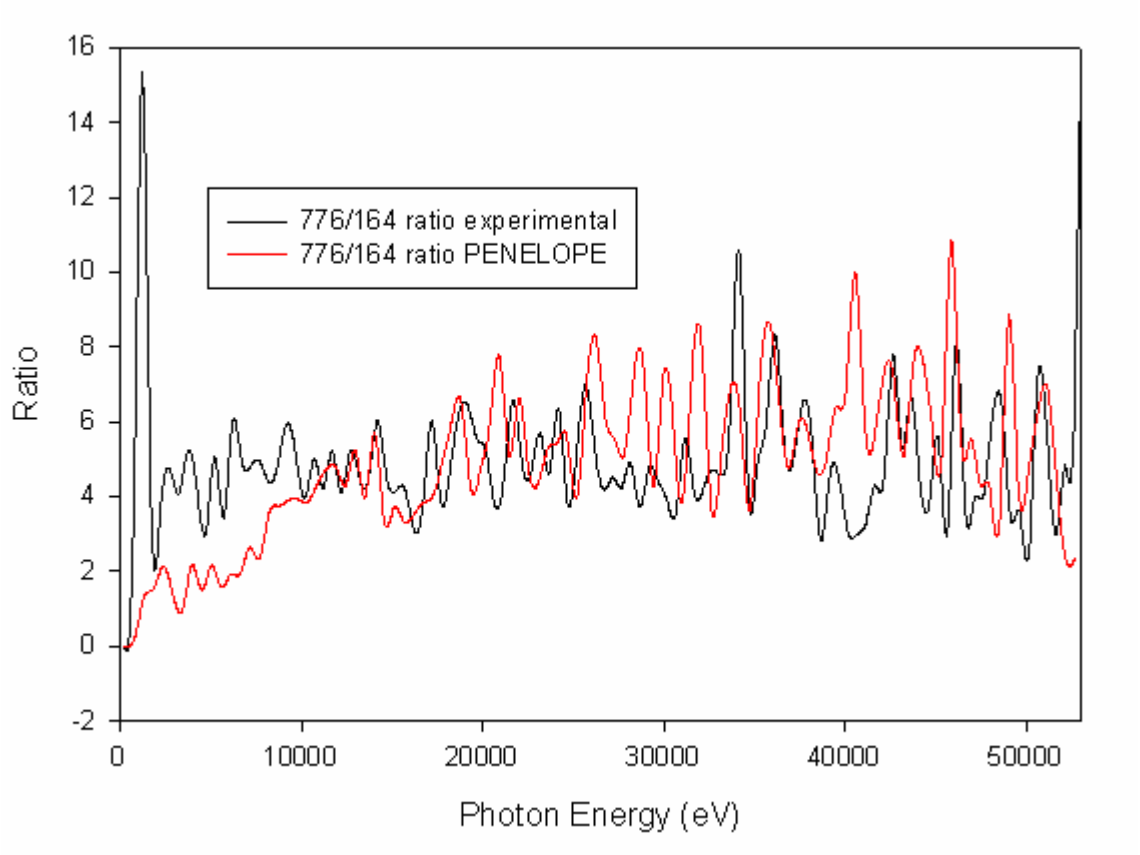

Figure 24 A comparison of the experimental and PENELOPE-generated ratios of the 776/164 μg/cm^2 target yields

Unlike the 135 degree data collected using the 549 μg/cm^2 film, the small pin-hole in the target doesn't seem to have much of an effect on the 90 degree data. This could be because the hole wasn't yet present when the 90 degree experiments were performed (the experiments featuring the 135 degree angle between the beam-line and the detector were performed after the 90 degree experiments), or it could simply be because the effective hole size is smaller when the target is positioned at an angle in relation to the electron beam.

A comparison of the experimental ratio of the 40978 μg/cm^2 and 5255 μg/cm^2 (the effective target thicknesses of the 28976 and 3716 μg/cm^2 films at 90 degrees) target yields to the corresponding PENELOPE-generated ratio is shown as a function of photon energy in Figure 25.

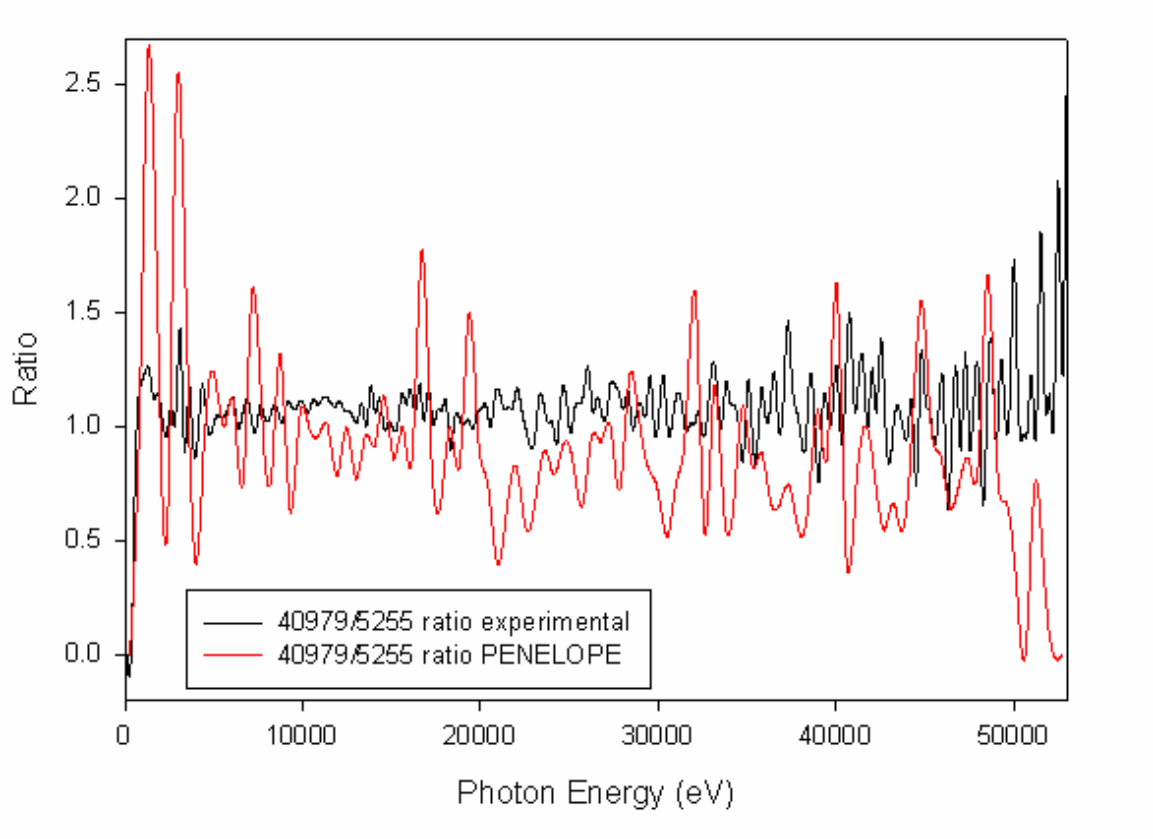

Figure 25 A comparison of the experimental and PENELOPE-generated ratios of the 40979/5255 μg/cm^2 target yields

While the overall shapes of the spectra are in relatively good agreement, the magnitudes are not. The PENELOPE-generated data ratio is significantly lower than the experimental data ratio. The PENELOPE ratio value (averaged over the entire energy range) is .891, and the experimental ratio value (also averaged over the entire energy range) is considerably higher (considering the excellent statistics) at 1.085. This indicates that PENELOPE predicts a higher yield for the 5255 μg/cm^2 film than it does for the

(thicker) 40979 μg/cm^2 film. Although the reason for this discrepancy has already been discussed, this comparison was included to demonstrate exactly how the difference in set-ups affects the data. Note that the PENELOPE ratio goes to zero as the photon energy approaches the energy of the incident electrons. This is presumed to be due to the fact (previously detailed) that photons with energies near that of the electrons are produced as the electron first enters the target (i.e. at relatively "shallow" parts of the target), before the electron has lost a significant portion of its energy; thus, the PENELOPE set-up – which positions the target perpendicular to the beam-line, and parallel to the area "seen" by the Ge detector – is such that the photons produced at these higher energies are under-represented in the simulation.

5.5 90 Degree Data Comparisons

Figures 26 through 28 are direct comparisons of the PENELOPE-generated and experimental data. As with the comparisons of the 135 degree data, both the efficiency and solid angle had to be taken into account when comparing the two 90 degree data sets. The efficiency was estimated using the same experimental efficiency measurements and XCOM efficiency data used in the 135 degree data comparisons, and the solid angle was once again measured using an Am 241 source. When dealing with the data sets, the yields were averaged over a 10 keV energy range (and plotted at the average energy) in order to improve statistics and decrease the amount of error. Note that (as before) only statistical error is represented in the error bars.

Figure 26 is a comparison of the experimental and PENELOPE-generated data (yields as a function of photon energy) for the 94 μg/cm^2 target (the effective target-thickness of the 66 μg/cm^2 film at 90 degrees).

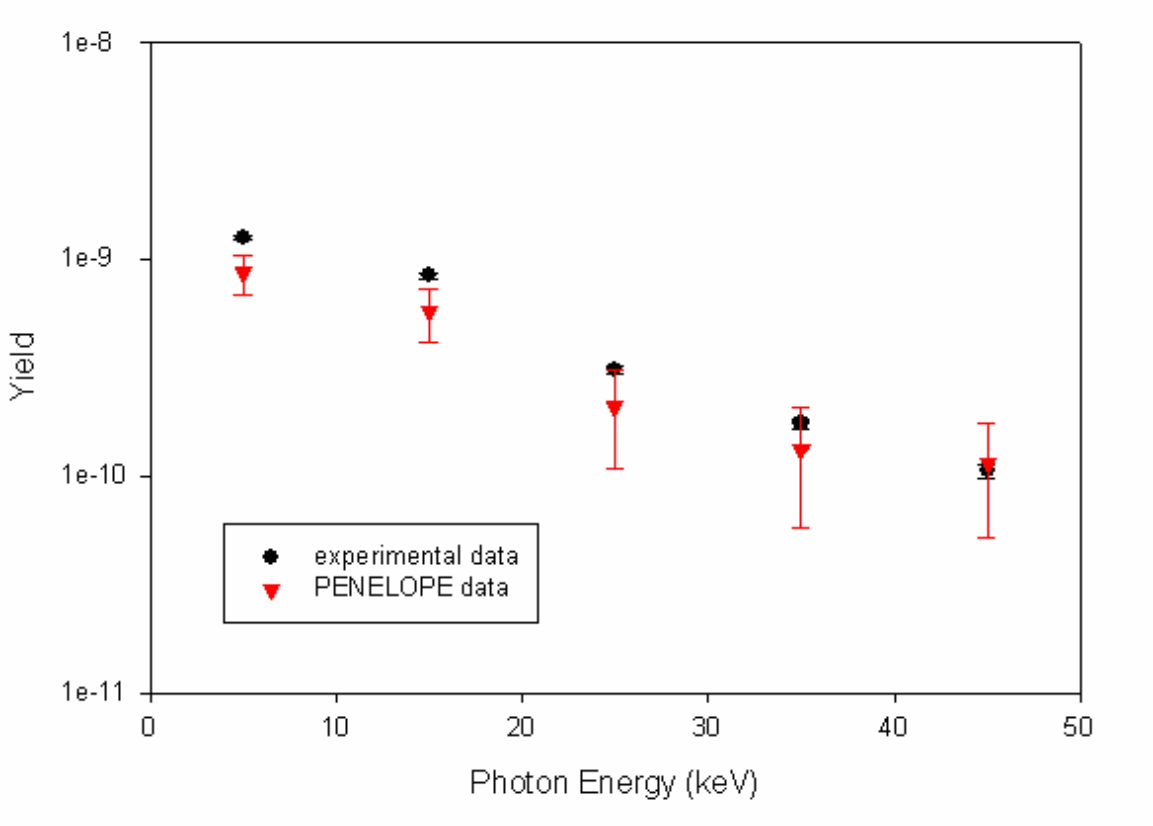

Figure 26 Plot of the experimental and PENELOPE-generated yields for the 94 μg/cm^2 target

The experimental and PENELOPE-generated yields agree with each other relatively well in both shape and magnitude. The PENELOPE yield seems to be slightly lower throughout most of the photon energy range (the lone exception being at 45 keV), and this could be due to the anticipated issue with the simulated PENELOPE set-up (detailed at the beginning of this section). It should be noted that this is in contrast to the 135 degree data comparisons, where the PENELOPE-generated yield was usually higher than the experimentally-obtained yield. The yields are most likely to agree for this target-

thickness, due to the fact that radiation absorption is at a minimum (compared to the other target-thicknesses featured). This figure does suggest, however, that – if not for the absorption issue introduced by the simulated set-up – our experimental yields would be in excellent agreement with the PENELOPE-generated yields for all target-thicknesses. However, even for this film (the thinnest one used in the experiments), the absorption issue can't be considered negligible.

Figure 27 is a comparison of the experimental and PENELOPE-generated data for the 164 μg/cm^2 target (the effective target-thickness of the 116 μg/cm^2 film at 90 degrees).

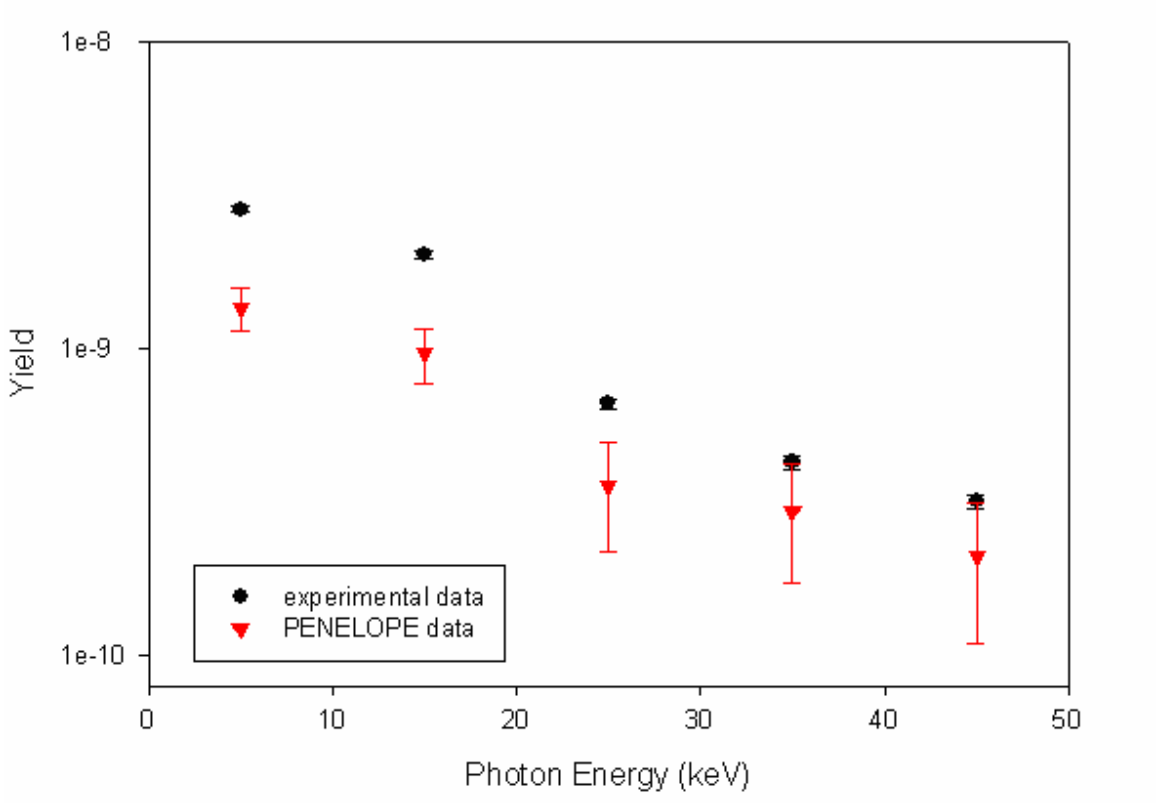

Figure 27 Plot of the experimental and PENELOPE-generated yields for the 164 μg/cm^2 target

In this figure, we can already see that the differences between the experimental and PENELOPE-simulated set-ups are an issue. The PENELOPE-generated yield is significantly lower than the experimental yield throughout the entire energy range, but the discrepancy is especially apparent at the low-energy end of the spectrum (where the absorption problem would affect the data most). It's interesting that we can already see significant disagreement between the experimentally-obtained and PENELOPE-generated yields, for films as thin as 164 $\mu g/cm^2$. This also helps us to understand why the averaged value of the PENELOPE-generated ratio for the 164 and 94 $\mu g/cm^2$ targets was less than the averaged value for the ratio of the experimentally-obtained data for the same two films (see Figure 23).

Figure 28 shows comparisons of the experimental and PENELOPE-generated yields for both the 5255 and 40979 $\mu g/cm^2$ targets (the effective target-thicknesses of the 3716 and 28976 $\mu g/cm^2$ films at 90 degrees). The two comparisons were plotted together in order to demonstrate what was hinted at in the ratio comparisons of the data for the two films: that the simulated (PENELOPE) set-up (erroneously) predicts a higher yield for the (thinner) 5255 $\mu g/cm^2$ film than for the (thicker) 40979 $\mu g/cm^2$ film due to the aforementioned affect of the absorption issue. The magnitudes of the PENELOPE-generated yields aren't even anywhere close to the magnitudes of the experimentally-obtained yields for these targets. The experimental data plots for the two targets are virtually identical, while the PENELOPE-generated data plots are quite different. It is interesting that PENELOPE predicts a lower yield at 5 keV than at 15 keV for both of the targets, and that the difference in the PENELOPE-generated yields grows as the photon

energy increases. The difference in the experimental and PENELOPE data, on the other hand, seems to decrease as photon energy increases.

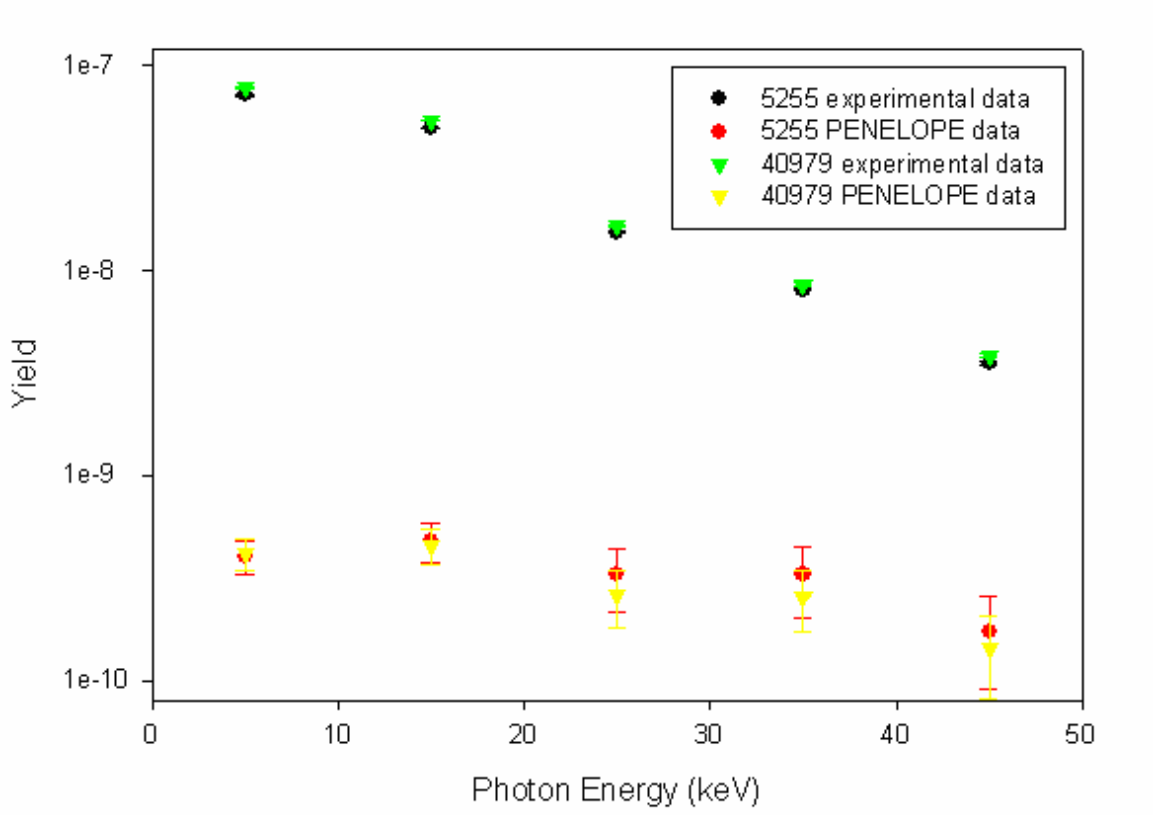

Figure 28 Plot of the experimental and PENELOPE-generated yields for the 5255 and 40979 μg/cm^2 targets

The discrepancies between the simulated data sets and the experimentally-obtained data sets in Figure 28 serve as testimony for the need to correct the PENELOPE code so as to accurately mimic the experimental set-up schematic shown in Figure 19.

5.6 Reflection/Transmission Comparisons

After reviewing the PENELOPE data, and taking into consideration its issues with absorption, we thought that it might be interesting to explore the effects of radiation

absorption through experiments involving comparisons of reflected and transmitted bremsstrahlung measured at 90 degrees from the electron beam-line. For the reflected radiation experiments, the familiar set-up shown in Figure 19 was employed, and for the transmitted radiation experiments, the set-up shown in Figure 29 was used. All data was normalized according to the amount of charge collected, and all background radiation (both natural and "stray electron") has been subtracted.

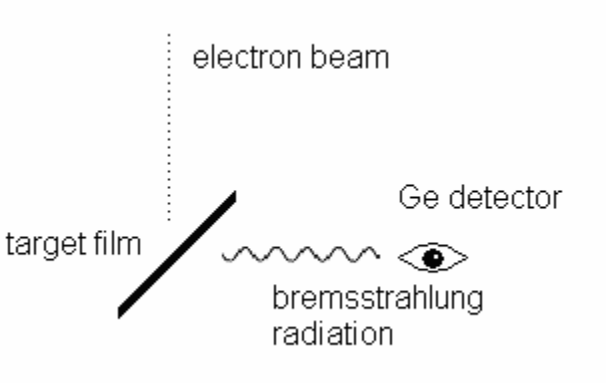

Figure 29 Diagram of the 90 degree transmission geometry used in the experiments

The first experiment was performed using the 94 μg/cm^2 film (effective thickness), and the radiation that was detected at an angle of 90 degrees from the beam-line (both transmitted and reflected) is represented in Figure 30. While the statistics could admittedly be stronger, the figure still clearly demonstrates that there is little difference in either the magnitude or shape of the radiation yields for the transmitted and reflected data. There seems to be little evidence of absorption affects.

The second experiment was performed using the 5255 μg/cm^2 film (effective thickness), and the results (both transmitted and reflected) are shown in Figure 31. This figure clearly shows a difference in the reflected and transmitted radiation. The yield for the transmitted radiation experiment is significantly lower than the yield for the reflected radiation experiment, especially in the 0 to 15 keV photon energy range. Note that the x-

ray peaks, however, seem to have the same magnitudes in both the reflected and transmitted plots.These figures were included in order to demonstrate the dependence of absorption on target-thickness.

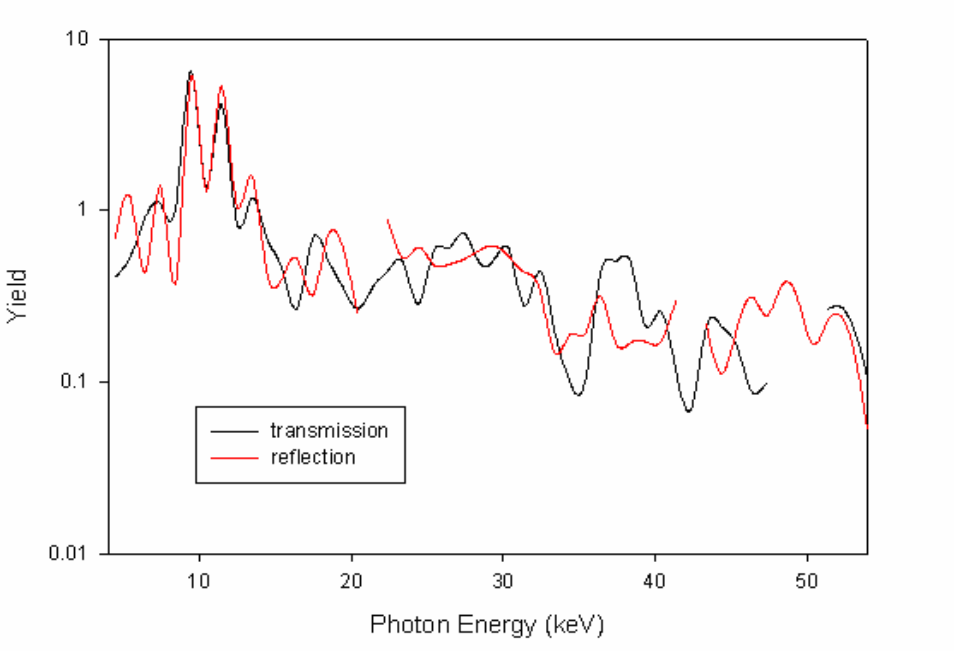

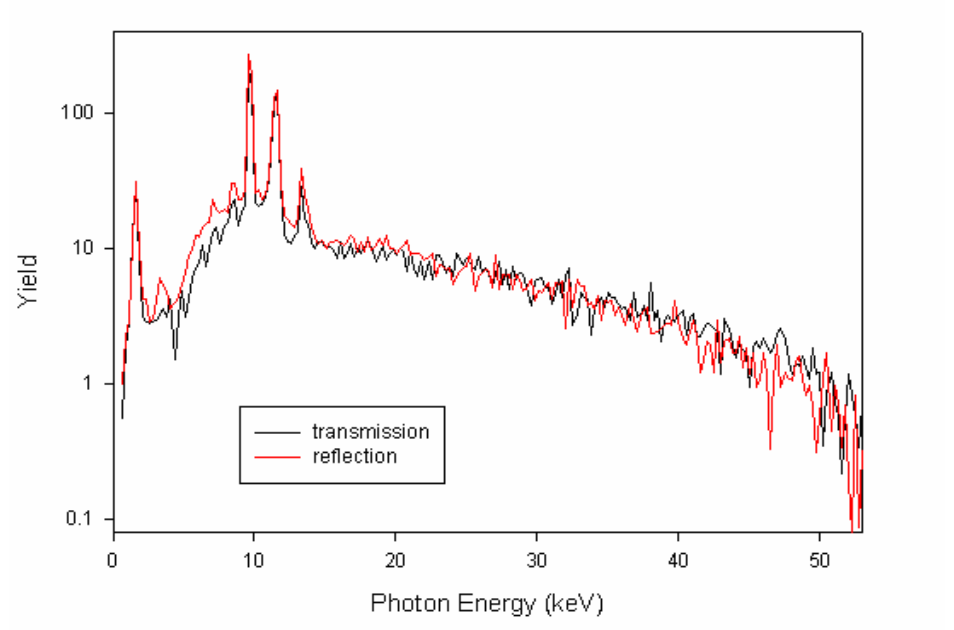

Figures 30 and 31 Comparisons of the 90 degree transmission and reflection yields for the 94 and 5255 μg/cm^2 targets as a function of photon energy

5.7 90 Degree Cross-Section Measurements

A plot of the absolute doubly-differential cross-section measurements for the 94 and 164 μg/cm^2 targets (effective thicknesses) as a function the energy of the photons produced in the experiments can be seen in Figure 32. As with the 135 degree cross-section measurements, the figure also includes theoretical predictions for both normal bremsstrahlung and the stripping approximation (where a polarizational bremsstrahlung contribution is included) for an infinitely thin gold film.

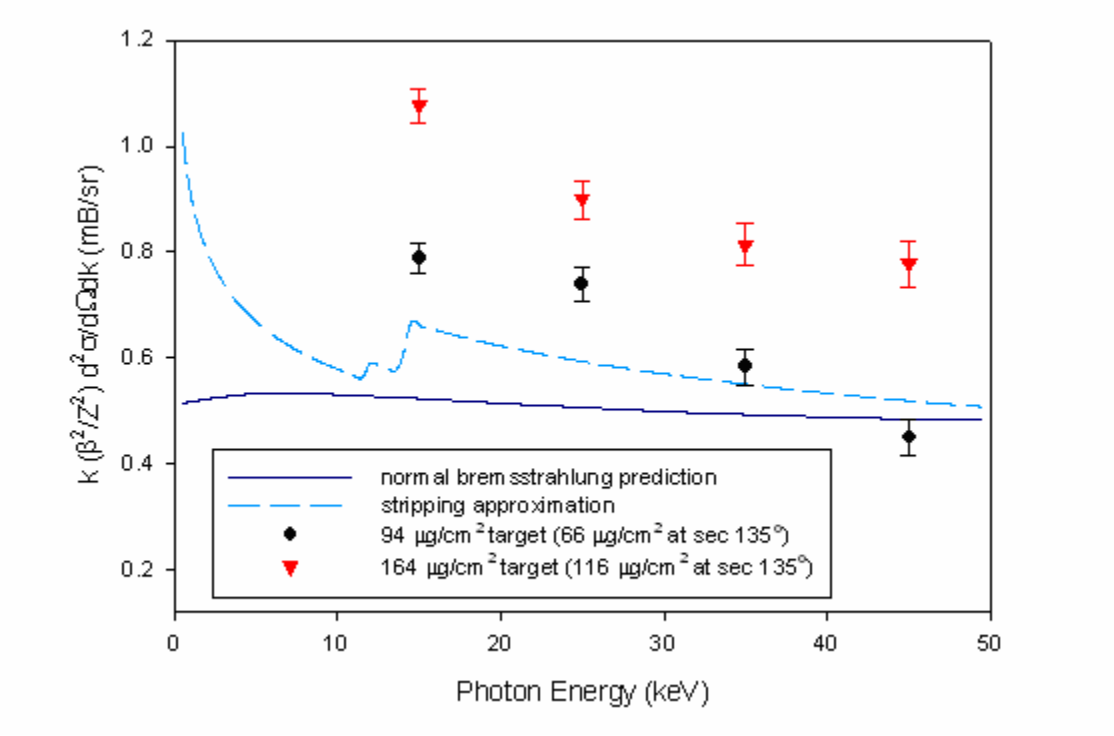

Figure 32 90 degree cross-section measurements as a function of photon energy for the 94 and 164 μg/cm^2 targets compared with the stripping approximation and normal bremsstrahlung predictions for an infinitely thin target

The doubly-differential cross-section values and the corresponding uncertainties are shown in Chart 3. The uncertainties shown are all purely statistical.

effective target thickness ($\mu g/cm^2$)	energy (keV)	DDCS measurement (mB/sr)	stat. uncertainty (mB/sr)	total uncertainty (mB/sr)
94	15	0.788	0.027 (3.5%)	0.043 (5.5%)
94	25	0.741	0.032 (4.3%)	0.044 (6.0%)
94	35	0.583	0.033 (5.6%)	0.041 (7.0%)
94	45	0.450	0.033 (7.2%)	0.038 (8.4%)
164	15	1.076	0.032 (2.9%)	0.055 (5.1%)
164	25	0.899	0.036 (4.0%)	0.052 (5.8%)
164	35	0.814	0.039 (4.8%)	0.052 (6.4%)
164	45	0.778	0.043 (5.5%)	0.054 (6.9%)

Chart 3 90 degree doubly-differential cross-section measurements and the corresponding uncertainties (both statistical and total) for the two thinnest targets

Cross-section measurements are given for both targets at energies of 25, 35, and 45 keV, along with a fourth (estimated) point at 15 keV. As with the 135 degree cross-sections, the 15 keV point was measured using only an estimate of the bremsstrahlung produced at this energy. The points in the figure represent the total bremsstrahlung radiation yield, summed over a 10 keV range, and plotted at the energy average of that range.

The 94 $\mu g/cm^2$ target (the effective thickness of the 66 $\mu g/cm^2$ film) cross-section measurements are somewhat surprising. The 15, 25 and 35 keV points are well above the normal bremsstrahlung prediction, while the 45 keV point is well below the normal bremsstrahlung prediction. As far as comparison with the stripping approximation is concerned, only one of the points (at 35 keV) is anywhere near agreement with the prediction, while the 15 and 25 keV points are significantly higher than the stripping approximation, and the 45 keV is significantly lower. While it wouldn't be surprising to find that a film with an effective target thickness of 94 $\mu g/cm^2$ can no longer be considered to be a "thin" film, and has a measured cross-section higher than the

prediction for an infinitely thin film, the slope of the plotted cross-section measurements is somewhat surprising.

The 164 μg/cm^2 target (effective thickness) cross-sections, shown in Figure 32, are higher than both the normal bremsstrahlung prediction and the stripping approximation.

This target clearly cannot be considered to be a true “thin” film. Comparison with theory indicates that a thickness of 164 μg/cm^2 is already thick enough that the single-interaction model is no longer adequate. The slope of the plotted points seems to be roughly the same as the slope of the 94 μg/cm^2 target cross-section measurements. Exactly why the slopes of the data for the 90 degree experiments are so different from the slopes of both the normal bremsstrahlung prediction and the stripping approximation isn’t completely understood.

5.8 Scattered Electron-Kapton Window Interactions

Initially, it was thought that the somewhat-surprising results shown in Figure 32 might be due to lower-energy background radiation. One possible reason for the slope of the plotted points and the disagreement with theory was thought to have something to do with scattered electrons striking the Kapton window. Comparing results for Kapton obtained using PENELOPE in conjunction with the Rutherford scattering cross-section to the gold-target yields obtained using PENELOPE and through experiment indicate that bremsstrahlung produced as a result of electrons scattered into the Kapton window contributes no more than about 1% to the overall spectrum, and mostly in the 0 to 15 keV

energy range. This effect, therefore, doesn't seem to be the cause of the discrepancy, and can be considered negligible.

The background produced from electrons scattering into the Kapton window is about three times smaller in magnitude for the 135 degree experiments, making it even less of a factor for the 135 degree data.

Another possible source of background radiation for the thin-target experiments would be from electrons scattered into the wall of the aluminum charge-collector. While aluminum is of a higher Z-value than Kapton (13 for aluminum, while the effective Z-value is a little over 6 for Kapton Polymide), the solid angle involved would make the background effects roughly comparable. Background radiation produced by electrons scattered by the aluminum charge-collector would be more of an issue for the 135 degree experiments than it would for the 90 degree experiments, due to the geometries of the set-ups.

VI. Error Analysis

One of the principle objectives of this study was to significantly improve upon the accuracy of the doubly-differential cross-section measurements done by other groups by significantly reducing the error in the measurements. This was mostly achieved through the reduction in the uncertainty of the target-thickness measurements (a result of our new way of measuring the thicknesses).

6.1 Error in Target-Thickness

As previously mentioned, the dominant source of error in our target-thickness measurements is the uncertainty in the absorption coefficient. The error in the coefficient was estimated to be about 3 percent. This estimate was based on a comparison of the XCOM and FFAST coefficients, which agree with each other for our application within about 3 percent; thus, we thought it reasonable to assume that the error on the coefficient itself was comparable. The remainder of the error in the target-thickness measurements is statistical error, a contribution which is minimal. The largest percent error in any of the thickness measurements was 3.1 percent (for the thinnest film measured). Compared with earlier experiments, where the error in target-thickness was more than 20 percent, this is a significant improvement.

6.2 Error in Photon Counts

The number of photon counts at photon energy k, N(k), is another factor that contributes to the overall error in the cross-section measurements. All error for this value

is purely statistical. While it may seem like this error can easily be reduced simply by running the experiments for a longer period of time (more charge), it is important to keep in mind that these experiments can take a *very* long time to run (especially for the thin-film experiments). The goal, as the experiments were being performed, was to keep the statistical error for N(k) below 10 percent. The largest percent error for any of the N(k) values was 9.7 percent for the cross-section measurement of the 45 keV data point for the 116 $\mu g/cm^2$ target taken at 135 degrees. The average percent error for the N(k) values was just a little over 6 percent.

6.3 Error in Solid Angle

The error in the measured solid angle, $\Delta\Omega$, is a result of both statistical error and error in the decay-rate of the source used in the measurements. Solid angle measurements were made using an Am-241 source over a 24-hour time period. Separate measurements were made for both the 90 and 135 degree set-ups. At date of manufacture, the National Bureau of Standards states that the Am-241 source has a total error of 1.9 percent. The percent error in the solid angle measurement for the 135 degree set-up was 2.1 percent, and the error in the solid angle measurement for the 90 degree set-up was also around 2 percent. There is also a small amount of error in the measured solid angle that results from systematic error from the uncertainties in the measurement of things such the size of the hole in the Pb collimator. These measurements were made using calipers with precisions of at least 1 mil, and it is assumed that this error contributes little to the net error (and is thus considered negligible). It wasn't necessary to consider the efficiency of

the Ge detector while making the measurements, due to the fact that detector efficiency is figured into the cross-section measurements independently.

6.4 Error in Detector Efficiency

The Ge detector's efficiency, $\varepsilon(k)$, is another factor that contributes to the overall error in the cross-section measurements. As detailed in Appendix C, there were several experimental measurements made in order to verify that the XCOM predictions for the Ge detector efficiency were accurate. These measurements proved the XCOM predictions to be reliable, and the XCOM data was used to estimate the detector's efficiency throughout the radiation energy range. Just as with the target-thickness measurements, the only factor to that really contributes to the error in our efficiency estimates would be the absorption coefficient (obtained from XCOM) for germanium. Once again, our error estimate was made using a comparison of the XCOM and FFAST coefficients for our particular application. The error in the coefficient was about 1 or 2 percent in the 10 to 50 keV energy range where are cross-sections were measured (the error is slightly higher < 10 keV). However, when computing the error in the efficiency, represented by the equation:

$$\varepsilon = 1 - e^{-\mu\tau}$$

where ε is the efficiency, μ is the absorption coefficient for germanium, and τ is the thickness of the germanium layer, the error resulting from the uncertainty in the absorption coefficient becomes negligible due to the exponential factor being nearly equal to zero throughout the relevant energy range. For similar reasons, the error in thickness can also be considered to be negligible. Taking these points into consideration,

the best way to estimate the error in our efficiency estimates is probably to compare them against theoretical predictions. Comparisons of our experimental data (with our efficiency estimates figured in) to PENELOPE-generated data are in very good agreement, indicating that our efficiency estimates have an error of (at most) 2 or 3 percent.

6.5 Error in Number of Incident Electrons

The error in N_e, the number of incident electrons, is dependent upon a couple of things. The systematic error in the charge collection is estimated to be around 1 percent. The Ortec current integrator and counter were last calibrated in 2002 by Salvador Portillo using a Pico-Amp source with a stated calibration error of less than 1 percent [Portillo, 2002].

6.6 Estimate of Total Error

Taking all of these contributions to the net error into consideration, a reasonable estimate of the total error in our doubly-differential cross-section measurements would be no more than 7 or 8 percent.

VII. Conclusion

7.1 Conclusions

The comparisons of our experimental data to the data simulated by PENELOPE don't seem to indicate any polarizational bremsstrahlung contribution for solid-film targets. None of the 135 degree data seems to indicate any polarizational bremsstrahlung contributions. The 135 degree experimental data is in good agreement with the normal bremsstrahlung predictions of Kissel, Quarles, and Pratt [Kissel et al., 1983] (on which the PENELOPE is based) for all seven targets. The only notable discrepancy between experimental and simulation is at 5 keV, and it may indicate that our efficiency estimate at that point may not be as good as we first thought. The 90 degree cross-section measurements aren't quite as conclusive. The 164 $\mu g/cm^2$ target is definitely too thick to be considered "purely thin", so it's difficult to compare with theory. The 94 $\mu g/cm^2$ cross-section, on the other hand, is well below both the normal prediction and the stripping approximation at 45 keV, but well-above both at 15, 25, and 35 keV. The slope of the cross-section measurements could indicate some type of background that we failed to subtract from our data. Despite the fact that PENELOPE has been tested previously, our experimental data provides further evidence that PENELOPE can accurately provide simulated data for electron-atom collisions (it can simulate positron-atom collisions, as well).

The comparisons with PENELOPE simulations also indicate that our target-thickness measurement technique provides accurate results. The PENELOPE predictions proved to be fairly sensitive to target-thickness (especially for the thinner targets), and this sensitivity, in conjunction with the agreement of our direct yield-comparisons,

suggests that our target-thickness measurements are of good accuracy. This new method of thickness measurement also allowed us to greatly reduce the amount of error in our doubly-differential cross-section measurements. This was crucial due to the fact that the stripping approximation (which includes polarizational bremsstrahlung contributions) is only slightly higher than the normal bremsstrahlung prediction (when plotted), and accuracy is essential when trying to determine which one is in better agreement with our experimental results.

Our target-thickness measurements greatly decrease the amount of uncertainty in target thickness compared to previous experiments conducted here at TCU [Ambrose, 1987], and this improves the accuracy of our doubly-differential cross-section measurements. In the past, there was as much as 20% error in the target-thickness measurements, and the largest error in any of the thickness measurements presented in this paper was only about 2%. This improvement in thickness measurement also allowed us to observe and study the transition from thin to thick-film spectra with greater confidence in our data.

The new-and-improved experimental set-up also allowed us to make more certain charge-collection measurements, and allowed us to obtain data at both 135 and 90 degrees.

7.2 Suggestions for Future Work

While the arguments against any polarizational bremsstrahlung contributions for solid-film target data presented in this work are convincing, there is certainly much more research to be done in the field.

Firstly, the PENELOPE program needs to be modified in order to accurately compare its predictions to the data we obtained at 90 degrees from the electron beam-line. This is not as trivial a task as it might first seem, and we have plans to contact Salvat (the author of the program) about the matter.

Secondly, a more complete theoretical description of the processes involved in our experiments needs to be developed. Our experimental results suggest that the stripping approximation may not be an adequate theory, and a more refined theory would need to be developed in order to make more definitive statements concerning polarizational bremsstrahlung contributions to solid-film bremsstrahlung spectra. Unfortunately, most of the theories that exist at this time are for single atom-electron interactions, rather than for bremsstrahlung produced by an incident electron scattered by multiple atoms (an exception being work done by a group in Russia [Nasanov et al., 2006]). Essentially, there doesn't seem to be much motivation for further investigating the subject through experiment until adequate theory exists for comparison.

Thirdly, it would be a good idea to work with different targets. Obviously, a material with a high Z-value would be desirable, but it would also be important to choose a target material that remains sturdy even when in the form of a very thin film (for the sake of practicality and because very thin films are of the greatest interest to us). A material without characteristic x-ray peaks in the 0 to 10 keV range might also be interesting to use in conjunction with a radiation detector with good efficiency in that range, in order to study low-energy bremsstrahlung. It is in this region that there is the largest difference between the normal bremsstrahlung prediction and the stripping

approximation, so this would naturally be an interesting energy region to look at more closely.

It would also be interesting to study the angle-dependence of bremsstrahlung in greater depth, taking data at multiple angles. Even a cursory comparison of our 90 and 135 degree data clearly demonstrates that bremsstrahlung is angle-dependent, and this is certainly something worth investigating further.

Other possible suggestions for experiments include reproducing the experiments presented in this paper using positrons, rather than electrons, and studying the extent of polarizational bremsstrahlung for gas targets in greater detail.

Appendix A

Sample calculations

DDCS (45 keV cross-section for 66 μg/cm^2 target, 135 degree experiments)

$$(d^2\sigma/dkd\Omega) = (\beta^2/Z^2)\,[(k_{average}\,N(k))/(\tau\,\Delta k\,a(k)\,\Delta\Omega\,\varepsilon(k)\,N_e)]$$

$$= (.423^2/79^2)\,[(45 \times 132.24) / (2.03E17 \times 10 \times 1 \times 1.62E\text{-}4 \times .99 \times 2.99E12)]$$

$$= .176 \text{ mB/sr}$$

Target thickness (3716 μg/cm^2 target)

$$x = -\,1/\mu \ln [\, I(x) / I_o \,]$$

$$= -\,(4.34E\text{-}4)^{-1} \ln [240567 / 1206837]$$

$$= 3716 \text{ μg/cm}^2$$

Appendix B

Target descriptions

The thinnest film, advertised by MicroMatter as having a thickness of 50 μg/cm^2, was measured to be 66 μg/cm^2 thick using the x-ray absorption method. It was evaporated onto a glass slide and transferred onto the target-holder, and has no conductive adhesive applied to it to improve the electrical connection. It should be noted that evaporated gold films are notoriously "lumpy", and that – even when viewed with the unaided eye – irregularities in thickness of the 66 μg/cm^2 film can be seen. The x-ray absorption method of measurement simply gives us the *average* thickness of a certain film. It is assumed, however, that the distribution of irregularities in thickness is uniform enough, and that the size of the electron beam spot is large enough (~ 0.3 cm) is large enough, that the average thickness value can safely be used as the *effective* thickness value for our purposes.

The second-thinnest film, advertised by MicroMatter as having a thickness of 100 μg/cm^2, and measured to be 116 μg/cm^2 thick using the x-ray absorption method. It, too, was made via the aforementioned evaporation technique, and has no graphite conductive adhesive applied to it. When viewed with the unaided eye, the 116 μg/cm^2 film appears to be of a more uniform thickness than the 66 μg/cm^2 film (both films are transparent).

The third film measured was advertised by MicroMatter as having a thickness of 500 μg/cm^2, and measured to be 549 μg/cm^2 using the x-ray absorption method. It was evaporated onto a glass slide and transferred onto the target-holder, and has the aforementioned graphite conductive adhesive applied to it to aid the flow of charge and to keep the film attached to the target-holder (the thicker films have a tendency to become

detached from their holders). At some point after the first experiment conducted using the 549 $\mu g/cm^2$ film, the target developed a small hole (best described as a "pin hole") near the outer edge of the exposed portion of the target. The "stray electron" background radiation spectra indicate that the electron beam is well-centered on the target films, and it was initially assumed that the hole would have no significant effect on the results of the experiments. However, the size of the hole gradually increased (during the time interval in which the experiments using the film were performed), and some of the results (discussed in a later section of this paper) indicate that the pin hole may have had some effect on the results.

The fourth and fifth gold films measured were advertised by MicroMatter as having thicknesses of 900 and 1130 $\mu g/cm^2$, and the x-ray absorption measurements indicated actual thicknesses of 939 and 1295 $\mu g/cm^2$, respectively. Both films were created by MicroMatter using the evaporation method, and both films had small amounts of graphite conductive adhesive applied around the edges.

The sixth film measured was purchased from Goodfellow Cambridge Limited with an advertised thickness of 3860 $\mu g/cm^2$, and had a measured thickness of 3716 $\mu g/cm^2$. The rolled film was attached to the target-holder using graphite conductive adhesive, applied at the edges to help keep the film attached to the aluminum target-holder (and for charge-collection purposes).

The seventh film used in the experiments was also purchased as a rolled film from Goodfellow Cambridge Limited, and has an advertised thickness of 28976 $\mu g/cm^2$. This film's thickness prevented any radiation from being detected during x-ray absorption measurements (in other words, $I(x) = 0$), thus the advertised thickness remains the best

estimate we have of its true thickness. Fortunately, however, beyond the continuous slowing-down approximation (CSDA) range, the amount of bremsstrahlung radiation produced is relatively insensitive to the target film's thickness, therefore accuracy for measurements of films beyond this range is of lesser importance than it is for thinner films.

Appendix C

Efficiency

One factor that was important to consider during analysis of the experimental data was the efficiency of the Ge detector. In order to estimate the efficiency of the detector, several experiments were run by Michelle Prewitt using Am241, Ba133, Bi207, Co57, and Se75 calibrated radioisotope sources, and this experimental data was compared to various theoretical estimates of the efficiency of germanium detectors. The theoretical estimate that most closely matched the experimental data was based on a simple model that used absorption coefficients from the NIST XCOM database. Estimates were obtained from the XCOM database for photon absorption coefficients for Ge and the various absorbers in the path of the radiation including the .05 mm Kapton window, the air between the window and the detector, the detector Be window and the Ge dead-layer in the detector.

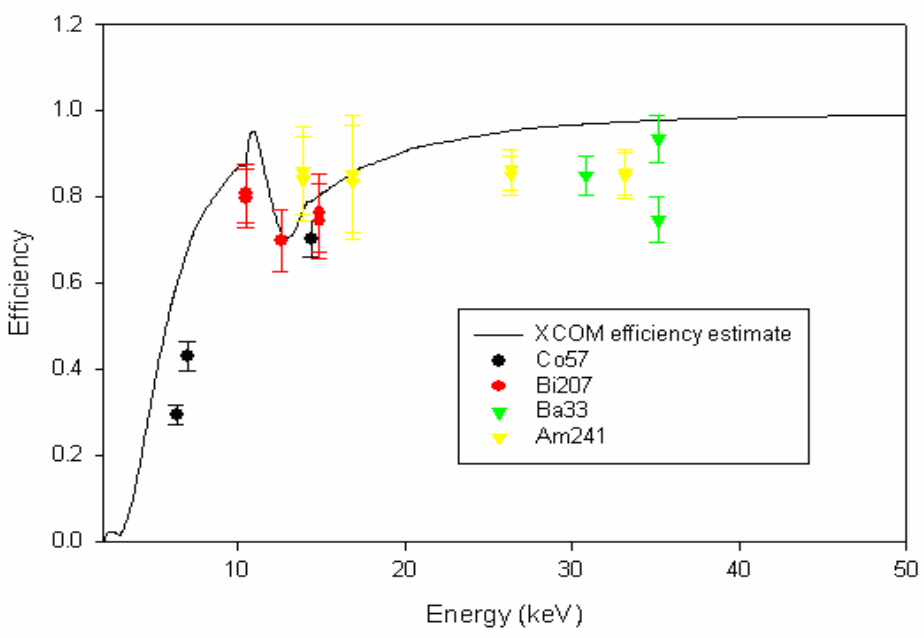

Figure 33 Comparison of the XCOM efficiency estimate for a Ge detector with experimental efficiency measurements using various calibrated radioisotope sources

Figure 33 is a plot of the experimental efficiency measurements (as well as the theoretical efficiency estimate based on the XCOM absorption coefficients) as a function of photon energy. Using the closest-matching theoretical estimate, we found that the average detector efficiency value was .61 from 0 to 10 keV, .84 from 10 to 20 keV, .94 from 20 to 30 keV, .98 from 30 to 40 keV, and .99 from 40 to 50 keV. These efficiencies were used when calculating the cross-sections and yields for all data presented in this work.

Glossary of Terms

$\varepsilon(k)$: efficiency of the Ge detector as a function of photon energy

k: photon energy

Δk: energy per channel

Normal bremsstrahlung: radiation emitted by a charged particle as it is scattered (accelerated) in a Coulomb field

N_e: number of incident electrons

N(k): photon counts at a particular energy

$\Delta\Omega$: solid angle

τ : target's thickness in atoms/cm^2

Polarizational bremsstrahlung: radiation emitted by atomic electrons as they are polarized by an incident charged particle

Thick-target bremsstrahlung: bremsstrahlung produced as a result of multiple scattering interactions per incident electron (prevalent in thick-film experiments).

Thin-target bremsstrahlung: bremsstrahlung produced as a result of a single scattering interaction per incident electron (prevalent in thin-target experiments)

References

Amusia, M. Ya., 2006. “Atomic Bremsstrahlung”: Retrospectives, current status and perspectives. Rad. Phys. And Chem. 75, 1232-1250

Ambrose, R., Altman, J.C., Quarles, C.A., 1987. Atomic-field bremsstrahlung cross-sections for incident electron energy from 50 to 100 keV for atomic numbers 6 to 92. Phys. Rev. A 35, 529-539

FFAST: http://physics.nist.gov/PhysRefData/FFast/Text/cover.html

Ishii, K., 2006. Continuous x-rays produced in light-ion-atom collisions. Rad. Phys. And Chem. 75, 1135-1163

Kissel, L., Quarles, C.A., Pratt, R.H., 1983. Shape functions for atomic-field bremsstrahlung from electrons of kinetic energy 1-500 keV on selected neutral atoms $1<Z<92$. Atom. Nucl. Data Tables 28, 381-460

Korol, A.V., Lyalin, A.G., Solovy’ov, A.V., Avbonia, N.B., Pratt, R.H., 2002. On the stripping approximation in the bremsstrahlung process. J. Phys. B 35, 1197-1210

Nasonov, N., Zhukova, P., 2006. Peculiarities in the low energy range of the bremsstrahlung spectrum. Rad. Phys. and Chem. 75, 1409-1429

Portillo, S., Quarles, C.A., 1999. Looking for polarizational bremsstrahlung in the midst of inner-shell ionization: Analysis of the x-ray spectrum in electron interactions with thin-film targets. Applications of Accelerators in Research and Industry CP475, 174-177

Portillo, S., 2002. Absolute doubly-differentail cross-sections from rare gas atoms. Ph.D. dissertation (Texas Christian University), unpublished

Portillo, S., Quarles, C.A., 2003. Absolute doubly differential cross-sections for electron bremsstrahlung from rare gas atoms at 28 and 50 keV. Phys. Rev. Lett. 91, 173201-1-173201-4

Pratt, R.H., Shaffer, C.D., Avdonina, N.B., Tong, X.M., Floresca, V., 1995. New developments in the theory of bremsstrahlung. Nucl. Inst. and Meth. in Phys. Res. B 99, 156-159

Quarles, C.A., 2000. Bremsstrahlung: An experimentalist's personal perspective on the postmodern era. Rad. Phys. and Chem. 59, 159-169

Salvat, F., Fernandez-Varea, J.M., Acosta, E., Sempau, J., 2001. The physics of electron/positron transport in PENELOPE. Proceedings of the Ninth EGS4 Users Meeting in Japan, KEK Proceedings 2001-22, 1-5

Salvat, F., Fernandez-Varea, J.M., Sempau, J., Llovet, X., 2006. Monte Carlo simulation of bremsstrahlung emission by electrons. Rad. Phys. and Chem. 75, 1201-1219

Verkhovtseva, E.T., Gnatchenko A.A., Zon, B.A., 2006. Resonance structures in polarizational bremsstrahlung from electron-atom collisions. Rad. Phys. and Chem. 75, 1115-1134

Wendin, G., Nuroh, K., 1977. Bremsstrahlung resonances and appearance potential spectroscopy near 3d thresholds in metallic Ba, La, and Ce. Phys. Rev. Lett. 39, 48-51

Williams, S., Haygood, R., Quarles, C.A., 2006. Target thickness dependence of bremsstrahlung from solid films. Rad. Phys. and Chem. 75, 1707-1710

Williams, S., Quarles, C.A., 2007. Target thickness dependence of 50 keV electron bremsstrahlung. Nucl. Inst. And Meth. in Phys. Res. B, in press

XCOM: http://physics.nist.gov/PhysRefData/Xcom/Text/XCOM.html

VITA

Scott Charles Williams was born April 30, 1980, in Fort Worth, Texas. He is the son of Pamela and Michael Williams. He received a Bachelor of Science degree with a major in physics from the University of North Texas in 2002, and a Master of Science degree with a major in physics from the University of Texas at Dallas in 2003. In January, 2004, he enrolled in graduate studies at Texas Christian University.

ABSTRACT

ABSOLUTE BREMSSTRAHLUNG YIELDS: 53 keV ELECTRONS ON GOLD

by Scott Williams
Department of Physics and Astronomy
Texas Christian University

Dissertation Advisor: Dr. C. A. Quarles, Professor

We report the results of our on-going study of the thickness-dependence of bremsstrahlung from solid gold film targets. The incident electrons' energy is approximately 53 keV, and we have collected data from angles of 90 and 135 degrees. Target thicknesses ranging from 66 μg/cm^2 (where single interaction conditions apply) to more than twice the electron range (where a multiple interaction model applies) were studied. With this data, we can observe the transition from thin to thick film spectra, and compare it to data obtained using the Monte Carlo simulation, PENELOPE. This comparison could reveal whether there is any polarizational bremsstrahlung contribution for solid film targets. We also present results for the absolute doubly-differential cross section for the thin-film targets and compare the results with predictions of both ordinary bremsstrahlung and total bremsstrahlung including a polarizational contribution calculated in the stripping approximation.